Open University of Cyprus

Faculty of Pure and Applied Sciences

Master of Science

Sustainable Energy Systems

Master Thesis

Stirling Engines for Low Temperature Solar Thermal Electric Power Generation

Author
Theodoros Diavatis

Supervisor Professor
Paris Fokaides

December 2019

Ανοικτό Πανεπιστήμιο Κύπρου

Σχολή Θετικών και Εφαρμοσμένων Επιστημών

Μεταπτυχιακό Πρόγραμμα Σπουδών

Sustainable Energy Systems

Μεταπτυχιακή Διατριβή

Stirling Engines for Low Temperature Solar Thermal Electric Power Generation

Όνομα Επώνυμο
Θεόδωρος Διαβάτης

Επιβλέπων Καθηγητής
Πάρης Φωκαίδης

Η παρούσα μεταπτυχιακή διατριβή υποβλήθηκε προς μερική εκπλήρωση των απαιτήσεων για απόκτηση μεταπτυχιακού τίτλου σπουδών
Στο ……..
από τη Σχολή Θετικών και Εφαρμοσμένων Επιστημών
του Ανοικτού Πανεπιστημίου Κύπρου.

Δεκέμβριος 2019

BLANK PAGE

Abstract

The subject of this master thesis is the design and development of a Stirling engine for low temperature solar thermal electric power generation. The purpose of the system is to incorporate low-cost materials and simple manufacturing processes while simultaneously increasing system performance. Studies, as well as existing Stirling systems applications, including several solar concentrators and Stirling engines/generators, presently and successfully demonstrate the technical feasibility of producing solar energy for extended periods of time. It is worth noting that because the solar-thermal technology is mature, the focus of this dissertation is the analysis, design and experimental assessment of low-temperature Stirling engine.

Reference is made to various solar thermal systems and to the different applications they find use. Consequently, different thermodynamic cycles are explained and analyzed in relation to the different thermodynamic systems in which they occur. In conclusion, Stirling engine is analysed. The engine is designed so that the working fluid is compressed in the colder part of the engine and expanded in the warmest part resulting in a clean conversion of heat to work. The key components of a Stirling engine are a heat source, a hot side heat exchanger, a regenerator, a cold side heat exchanger, a heat sink and a displacer. Stirling engines are categorized into three main types: a) the alpha, b) the beta, and c) the gamma configuration.

Blank Page

Symbols		
Name	**Symbol**	**Unit**
Engine pressure	P	Pa
Swept volume of expansion piston or displacer piston	V_{SE}	m^3
Swept volume of compression piston or power piston	V_{SC}	m^3
Dead volume of expansion space	V_{DE}	m^3
Regenerator volume	V_R	m^3
Dead volume of compression space	V_{DC}	m^3
Expansion space momental volume	V_E	m^3
Compression space momental volume	V_C	m^3
Total momental volume	V	m^3
Total mass of working gas	m	kg
Gas constant	R	J/kgK
Expansion space gas temperature	T_H	K
Regenerator space gas temperature	T_R	K
Compression space gas temperature	T_C	K
Phase angle	dx	deg
Temperature ratio	t	
Swept volume ratio	v	
Dead volume ratio	X	
Engine speed	n	Hz
Indicated expansion energy	W_E	J
Indicated compression energy	W_C	J
Indicated energy	W_i	J
Indicated expansion power	L_E	W
Indicated compression power	L_C	W
Indicated power	L_i	W
Efficiency	η	
Energy	E	J
Heat	Q	J
Temperature	T	K
Low temperature	T_L	K
High temperature	T_H	K

Table of Contents

List of Figures

List of Tables

Chapter 1

Introduction

Modern societies consume huge amounts of energy for heating buildings, transportation, electricity production and industrial use. Due to economic progress and a rising standard of living, the demand for energy is continually increasing. Nowadays, the largest amount of energy which is used is derived from fossil fuels, the continuous exhaustion of which has drawn a growing interest in renewable (inexhaustible) energy sources such as geothermal, tidal, hydroelectric, wind and solar. These have less impact to the environment than the traditional ones that have created various problems, the most serious of which is the greenhouse effect. It was reported that more than one third of energy consumption in the world that is used by industries about 20-50% is finally exhausted as the waste heat into atmosphere (Agency, 2018), (IPCC, 2018). Thus, by exploiting low grade temperature renewable heat resources, such as geothermal and solar energy provide us with significant opportunities for addressing energy related problems.

Another major problem with many renewable energy processes is that they are intermittent. Wind and solar electricity generation have been shown to have low capacity factors, 34.6% and 25.7% respectively in the US in 2017 (Administration, International Energy Outlook 2018, 2018), (Administration, Capacity Factors for Utility Scale Generators Not Primarily Using Fossil Fuels, 2018). Without energy storage methods, these processes have difficulty replacing conventional baseload energy generation processes that have higher capacity factors, such as natural gas, 51.3% , and coal, 53.7%, (Administration, Capacity Factors for Utility Scale Generators Not Primarily Using Fossil Fuels, 2018), (R. Fares, 2015). Despite all the above solar energy is one of the more attractive renewable energy sources that can be used as an input energy source for heat engines.

Technologies that can produce electricity from a temperature difference include the organic Rankine cycle (ORC) (Kolin I., 1991), thermoelectric generators (TEG) (Gentherm, n.d.), and Stirling engines (Cool Energy Inc, 2016). Stirling engines because of their inherent simplicity requires no pumps, valves or turbines unlike the organic Rankine cycle (C. P. Speer, 2018). The TEGs are further simpler than the Stirling engine. However, there maximum thermal efficiencies are dependent on both the materials used and the temperature of the thermal source and sink. Since all heat engines operate from a temperature difference between a heat source and the sink to produce power, if the heat source temperature is fixed, then the lowest thermal sink temperature is desired. In most cases, the thermal sink used to reject heat is the ambient air.

Due to their capabilities and high efficiencies, Stirling cycle engines have attracted increasing attention in recent decades. Stirling engine has the potential to be much more efficient than a gasoline or diesel engine. They operate with a closed regenerative thermodynamic cycle that has the same theoretical thermal efficiency of the Carnot cycle which is the highest one that can be achieved from a thermal engine. The compressible working fluid in a Stirling cycle could be for example air, helium, hydrogen, nitrogen, etc. The fluid medium experiences periodically compression and expansion at different temperature levels to convert thermal energy into mechanical work. The lack of valves and absence of periodic explosions in Stirling cycle engines enable them to be operated more quietly than other piston engines. Although, the Stirling cycle engine is classified as an external combustion engine the thermal energy can also be supplied by non-combusting sources such as solar or nuclear energy. Therefore, they have a great flexibility to be powered by any kind of heat sources at any temperature levels. The Stirling cycle engines working at low and moderate temperatures with simple constructions and low costs have a wide application prospect for recovering small-scale distributed low-grade thermal energy.

Direct solar-powered Stirling engines may be of great interest to countries where solar energy is available in unlimited quantity. To use direct solar energy, a solar concentrator and absorber must be integrated with the engine system. The solar radiation can be focused onto the displacer hot-end of the Stirling engine, thereby creating a solar-powered prime mover. The direct conversion of solar power into mechanical power reduces both the cost and complexity of the prime mover. Since during two-thirds of the day, solar energy is not available, solar/fuel hybrids will be needed. For solar electric

generation in the range of 1–100 kWe, the Stirling engine was considered to be the cheapest. Although the efficiency of a Stirling engine may be low, reliability is high and costs are low, which are the keys to a cost-effective Stirling solar generator.

1.1. Thermodynamic Cycles

The Stirling engine is a closed-cycle thermal regeneration engine with a gas operating fluid. The closed-cycle in this context, means a thermodynamic system. Furthermore, devices or systems used to produce net power output are often called engines, and the thermodynamic cycles in which they operate are called power cycles.

Depending on the phase of the working fluid, a thermodynamic cycle can be categorised as gas cycle or vapour cycle. In a gas cycle, the working fluid remains in the gaseous phase throughout the cycle. Instead, in a vapour cycle, the working fluid changes phase from vapour to liquid during the process. In addition, thermodynamic cycles can be also categorised in closed and open cycles. In closed cycles, the working fluid is returned to the initial state at the end of the cycle and is recirculated. In open cycles, the working fluid is renewed at the end of each cycle instead of being recirculated.

The most well-known thermodynamic cycles are listed below:

- Carnot;
- Otto;
- Diesel;
- Ericsson;
- Stirling;
- Brayton;
- Rallis (is analysed in a separate chapter)

The **Carnot** cycle is a cycle that can be operated in a closed system (i.e. piston-cylinder assembly) or in a steady-flow system (i.e. utilizing two turbines and two compressors). The cycle consists of four fully reversible processes, isothermal heat addition (1→2), isentropic expansion (2→3), isothermal heat rejection (3→4) and isentropic compression (4→1). Figure 1 below, shows the P-V and T-S diagrams of Carnot cycle.

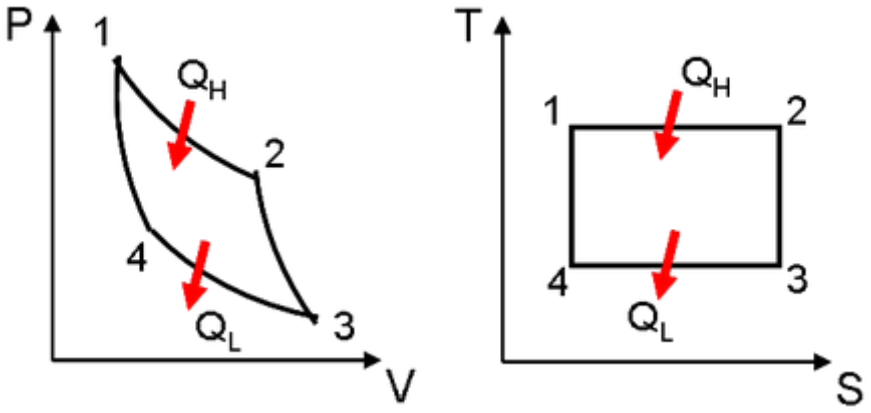

Figure 1. P-V and T-S diagrams of Carnot Cycle.

The Carnot cycle is the most efficient cycle that can be used between a heat source at temperature T_H and a sink at temperature T_L, and its thermal efficiency is given by the equation below:

$$\eta_{th,Carnot} = 1 - \frac{T_L}{T_H} \quad (1)$$

The **Otto** cycle is the most commonly used cycle in automobile engines. The cycle is ideal for spark-ignition reciprocating engines. An ideal Otto cycle consists of four internally reversible processes, the isentropic compression (1→2), the constant-volume heat addition (2→3), the isentropic expansion (3→4) and the constant-volume heat rejection (4→1). Figure 2 below shows the P-V and T-S diagrams of an ideal Otto cycle.

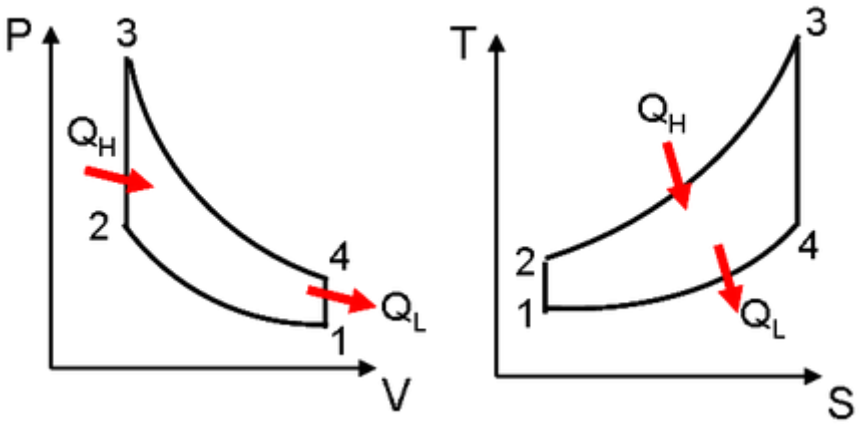

Figure 2. P-V and T-S diagrams of ideal Otto cycle.

The thermal efficiency of the ideal Otto cycle is given by the equation below:

$$\eta_{th,Otto} = 1 - \frac{1}{r^{k-1}} \quad (2)$$

Where:

r: is the compression ratio V_{max}/V_{min}

k: is the specific heat ratio c_p/c_v.

The **Diesel** cycle is the ideal cycle for compression-ignition (CI) engines. A CI engine is a reciprocating internal combustion engine. In compression-ignite engines the air is compressed at a temperature that exceeds the auto ignition temperature of the fuel and the combustion starts on contact as the fuel is introduced into that hot air. An ideal Diesel cycle consists of four distinct processes, isentropic compression of the fluid (1→2), and reversible constant pressure heating (2→3), isentropic expansion (3→4) and reversible constant volume cooling (4→1). Figure 3 below shows the P-V and T-S diagrams of an ideal Diesel cycle.

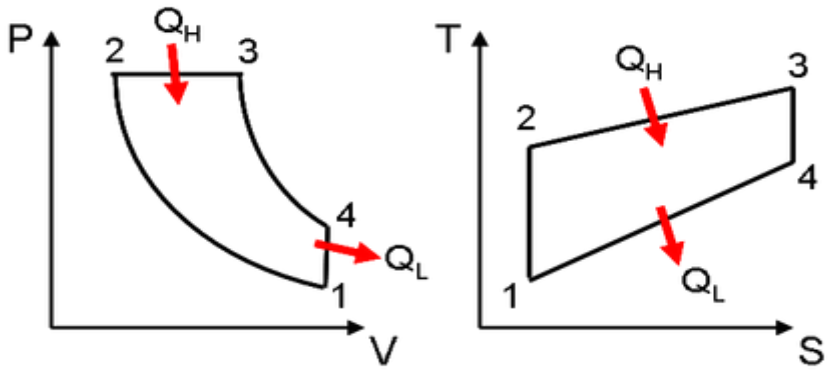

Figure 3. P-V and T-S diagrams of ideal Diesel cycle.

The thermal efficiency of a Diesel cycle is inversely proportional to compression ratio r and is given by the equation below:

$$\eta_{th,Diesel} = 1 - \frac{1}{r^{\gamma-1}}\left(\frac{\alpha^{\gamma} - 1}{\gamma(\alpha - 1)}\right) \quad (3)$$

Where:

r: is the compression ratio V_1/V_2

γ: is the ratio of specific heats c_p/c_v

α: is the cut-off ratio V_3/V_2

The **Ericsson** cycle is a cycle that involves an isothermal heat-addition process at T_H and an isothermal heat-rejection process at T_L. The difference between an Ericsson and a Carnot cycle is that the two isentropic processes in the Carnot cycle are replaced by two constant-pressure regeneration processes in the Ericsson cycle. Therefore, an Ericsson cycle uses regeneration, a process in which heat is transferred to a thermal energy storage device during part of the cycle and transferred back to the working fluid during another part of the cycle. In an ideal Ericsson cycle occur four processes, an isothermal compression (1→2), isobaric heat addition (2→3), isothermal expansion (3→4), and isobaric heat removal (4→1). Figure 4 below shows the P-V and T-S diagrams of an ideal Ericsson cycle.

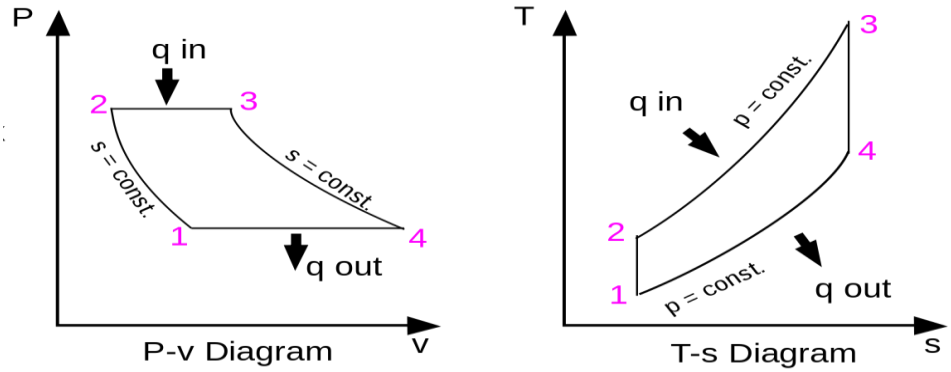

Figure 4. P-V and T-S diagrams of ideal Ericsson cycle.

Because, the Ericsson cycle is totally reversible, its thermal efficiency (for an ideal cycle) is given by the same equation as in the Carnot cycle, thus:

$$\eta_{th,Ericsson} = 1 - \frac{T_L}{T_H} \tag{4}$$

The **Stirling** cycle is also a cycle that involves an isothermal heat-addition process at T_H and an isothermal heat-rejection process at T_L. It differs from the Ericsson cycle in that the two constant-pressure regeneration processes are replaced by two constant-volume regeneration processes in the Stirling cycle. In an ideal Stirling cycle, the same four processes occur as in an Ericsson cycle. Figure 5 below shows the P-V and T-S diagrams of an ideal Stirling cycle.

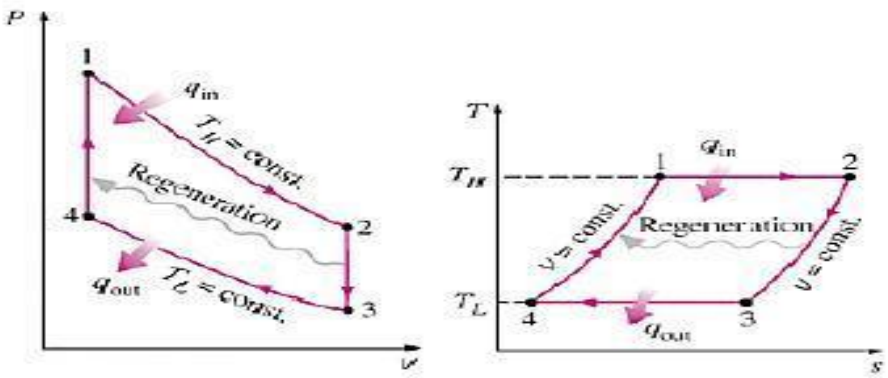

Figure 5. P-V and T-S diagrams of ideal Stirling cycle.

$$\eta_{th,Ericsson} = 1 - \frac{T_L}{T_H} \tag{5}$$

Finally, the **Brayton** cycle is an open-cycle. It is used mostly in gas turbines that both the compression and the expansion processes take place in the rotating machinery. The ideal Brayton cycle is made up of four internally reversible processes, the isentropic compression (in a compressor) (1→2), constant-pressure heat addition (2→3), isentropic expansion (3→4) and constant-pressure heat rejection (4→1). Figure 6 below shows the P-V and T-S diagrams of an ideal Brayton cycle.

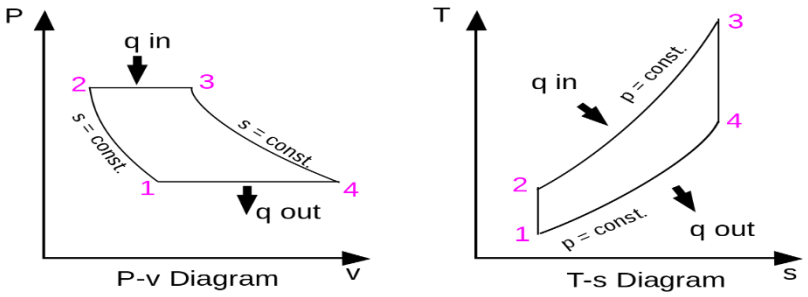

Figure 6. P-V and T-S diagrams of ideal Brayton cycle.

The thermal efficiency of a Brayton cycle is given by the equation below:

$$\eta_{th,Brayton} = 1 - \frac{1}{r_p^{\frac{(k-1)}{k}}} \tag{6}$$

Where:

r_p: is the pressure ratio P2/P1

k: is the specific heat ratio

Chapter 2

The Low Temperature Difference (LTD) Stirling Engine

The low-temperature differential (LTD) Stirling engine is a type of Stirling engine that can run with a small temperature difference between the hot and cold ends of the displacer cylinder. It is therefore able to operate with various low-temperature heat sources. Most kinetic LTD Stirling engines are implemented in a gamma configuration and driven by the crank-slider or Ringbom drive mechanism.

Some characteristics of the LTD Stirling engine are:

i. High compression or volume ratio (displacer to power-piston),
ii. Operate at low speeds,
iii. The diameter of the displacer cylinder is usually large; its length is often very short and its stroke is small too,
iv. They use annular gap between displacer and cylinder rather than porous media as regenerator,
v. The dwell period at the end of the displacer stroke is slightly longer than the normal Stirling engine,
vi. The heat exchangers tend to have large surface areas for heat transfer,

Although, Stirling engine has been studied by a large number of researchers, the LTD Stirling engine has received comparatively little attention. The efforts to reduce the temperature difference that a Stirling engine could operate off started in 1975 by Haneman (Haneman D., 1975) and led by Kolin (Kolin I., 1991) and Senft (Senft J., A simple derivation of the generalized Beale number, 1982), (James R. Senft, 1993). Haneman constructed an unusual engine using air with low-temperature sources, in

which the exhaust heat was still sufficiently hot to be useful for other purposes. In 1980, invented a gamma-type Stirling engine that could run off a temperature difference of 44 °C. A simply constructed low-temperature heat engine modelled on the Stirling engine configurations was patented by White (White E.W, 1983) in 1983. White suggested improving performance by pressurizing the displacer chamber. Efficiencies were claimed to be around 30%, which is regarded as quiet high for a low-temperature engine. O'Hare (O'Hare L.R., 1984) in 1984 patented a device which passed cooled and heated streams of air through a heat exchanger by changing the pressure of air inside the bellows. The practical usefulness of this device was not shown in detail as in the case of Haneman's work. Spencer (Spencer L.C., 1989) in 1989 reported that, in practice, such an engine would produce only a small amount of useful work relative to the collector system size, and would give little gain compared to the additional maintenance required.

From 1980 to 1991 the temperature difference between the two mediums was driven even lower than 44 degrees and the record of the engine to operate off the lowest temperature difference passed between Senft and Kolin. After the pioneering work of Kolin and Senft, various model engines have been developed and even commercialized for demonstration and teaching purposes. In general, the commercial small LTD Stirling engine models typically have power output in the order of 1 to 10 mW, speed under 500 rpm with thermal efficiencies below 0.1% (Aragn-Gonzlez G, 2013). Finally, in 1991, Senft (Senft J.R., An ultra low temperature differential Stirling engine, 1991) was able to produce an engine that ran off with an ultra-low temperature difference of 0.5^{o}C. It has been very difficult for anyone to create an engine with a result better than this. All the LTD Stirling engines developed by Senft and Kolin were gamma-type, and used flat plate heat exchangers. Senft (Senft J.R., Ringbom Stirling Engines, 1993) described the design and testing of a small LTD Ringbom Stirling engine powered by a 60 degrees conical reflector. He reported, that with the above reflector, the engine produced a hot end temperature of 93^{o}C under running conditions and worked very well. Rizzo (Rizzo J.G., 1995) reported that Kolin experimented with 16 LTD Stirling engines, over a period of 12 years. Kolin presented a model that worked on a temperature difference between the hot and cold ends of the displacer cylinder which was as low as 15^{o}C. Iwamoto et al. (Iwamoto I. Toda F. Hirata K. Takeuchi M. Yamamoto T., 1997) compared the performance of a LTD Stirling engine with a high-temperature differential Stirling

engine. They concluded that the LTD Stirling engine efficiency at its rated speed was approximately 50% of the Carnot efficiency. However, the compression ratio of their LTD Stirling engine was approximately equal to that of a conventional Stirling engine. Its performance, therefore, seemed to be the performance of a common Stirling engine operating at a low operating temperature.

Kongtragool and Wongwises (Kongtragool B. Wongwises S., Theoretical investigation on Beale number for low temperature differential Stirling engines, 2003) reviewed and discussed the available formulas for calculating the power output of Stirling engines, including Malmo formula (Reader G. Hooper C., 1983), Schmidt formula (Schmidt G., 1871), West formula (West CD., 1986), Beale formula (Reader G., 1983), and mean pressure power formula (Walker G., 1979), (West C., 1981), (Senft J., A simple derivation of the generalized Beale number, 1982). It is concluded that the mean pressure power formula is the most appropriate and simplest for estimating the power output of a gamma type configuration of LTD Stirling engine. Later in 2005 the same authors pointed out that the mean-pressure power formula was the most appropriate for LTD Stirling engine power output estimation. However, the hot-space and cold-space working fluid temperatures were needed in the mean-pressure power formula. Kongtragool and Wongwises (Bancha Kongtragool, 2005) presented the optimum absorber temperature of a once-reflecting full-conical reflector for a LTD Stirling engine.

A mathematical model for the overall efficiency of a solar-powered Stirling engine was developed and the limiting conditions of both maximum possible engine efficiency and power output were studied. Results showed that the optimum absorber temperatures obtained from both conditions were not significantly different. Furthermore, the overall efficiency in the case of the maximum possible engine power output was very close to that of the real engine of 55% Carnot efficiency. Kongtragool and Wongwises (Kongtragool B., 2007), also reported the performance of two LTD Stirling engines tested using LPG gas burners as heat sources. The first engine was a twin-power-piston engine and the second one was a four power-piston engine. Engine performances, thermal performances, including the Beale's numbers were presented.

2.1. Stirling Engine Configurations

Stirling engines can be divided into four main categories: alpha, beta, gamma and free piston configurations. There are also other obscure types of engine such as the thermoacoustic and the fluidyne engine which will not be discussed here.

2.1.1. Alpha (α) Stirling Configuration

The alpha type configuration of a Stirling engine uses two power pistons connected in series by a cooler, a regenerator and a heater. It has two cylinders, the compression space (cold temperature source) and expansion space (hot temperature source). It is a mechanically simple engine and typically produces a high power-to-volume ratio, however there are often problems related to the sealing of the expansion piston under high temperatures. The alpha engine shown in Figure 1 is a horizontally opposed type, which has the smallest dead space but requires rather length and complicated linkages to join the pistons to the crankshaft. Another variant is the 'V' design where both pistons are arranged in a V formation and are attached at a common point on the crankshaft. This means the heater and cooler are separated which reduces thermal shorting losses. However it increases dead space through the need to have an interconnecting passageway, containing the regenerator, between them. This design lends itself well to the double-acting configuration as pictured in Figure 2. In this configuration, there is only one piston per cylinder, but the space both in front and behind it form the expansion and compression spaces respectively. This type of engine was researched a lot by Philips from the 1940's until the 1960's and was quite successful, having a good power to weight ratio and capable of very respectable outputs.

Whereas early (1940s) double-acting air engines were said to have wobble-plate drive mechanisms the later (1960s) were described as having a swash-plate drive mechanism. A distinction between a swash-plate and a wobble-plate is sometimes hard to make. Maki et al. (1971) define a true swash-plate drive mechanism as one that features an inclined disk rigidly attached to the rotating shaft whereas the wobble-plate doesn't rotate with the shaft but merely rotates. In any event, Philips have adopted "swash-plate" to describe the drive on recent engines and, interestingly, retain the term "wobble-plate" for the older engines. Philips Type 4-65 DA engine was a four-cylinder

double-acting engine designed for 44 KW brake power (60 brake hp) and in 1973 was said by van Beukering et al. to have been running over 2000 hours on test. No other details of performance have been disclosed and the engine probably served as a workhorse for the development of subsequent engines of the same form but of larger capacity.

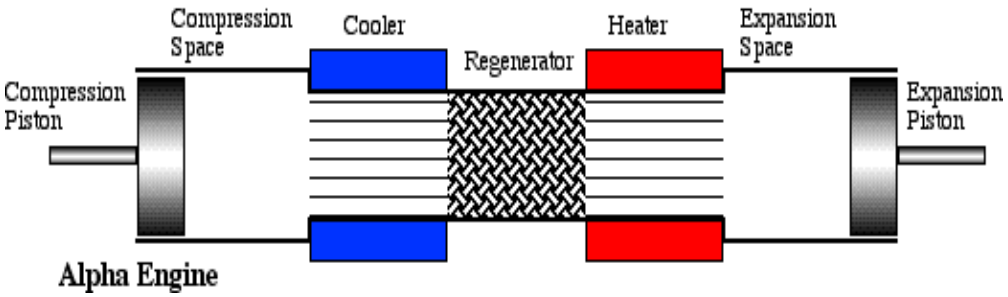

Figure 7. Alpha type Stirling engine (mechanical configuration).

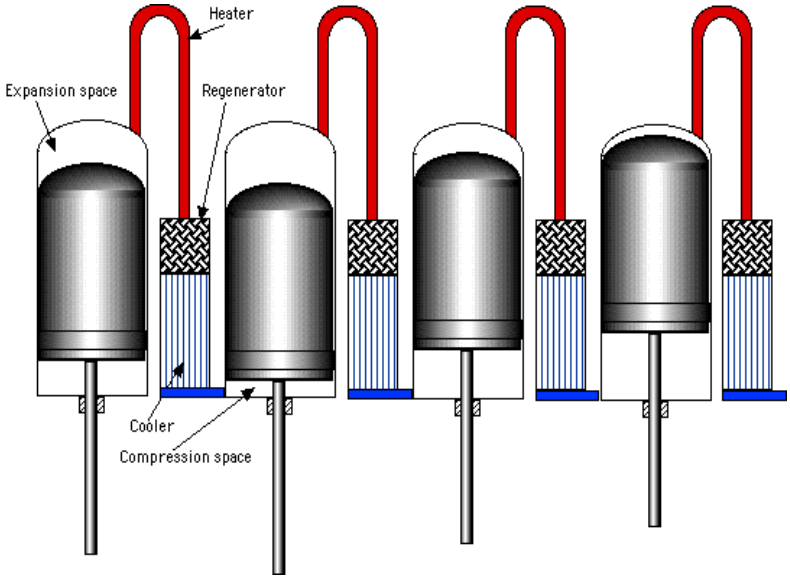

Figure 8. Four cylinder double-acting alpha type Stirling engine.

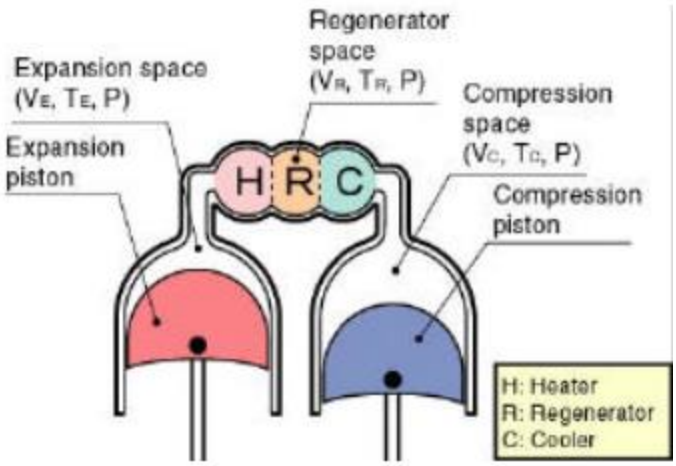

Figure 9. Schematic of alpha type Stirling engine.

The volumes of the expansion and compression cylinder at a given crank angle are determined at first. The instantaneous volumes is described with a crank angle - x. This crank angle is defined as x=0 when the expansion piston is located the most top position (top dead point). The instantaneous expansion volume - VE is described in equation (7) with a swept volume of the expansion piston - VSE, an expansion dead volume - VDE under the condition of assumption (g).

$$V_E = \frac{V_{SE}}{2}(1 - cosx) + V_{DE} \tag{7}$$

The instantaneous compression volume - VC is found in equation (2) with a swept volume of the compression piston - VSC, a compression dead volume - VDC and a phase angle - dx.

$$V_C = \frac{V_{SC}}{2}[1 - \cos(x - dx)] + V_{DC} \tag{8}$$

The total instantaneous volume is calculated in eq. (9)

$$V = V_E + V_R + V_C \tag{9}$$

By the assumptions (a), (b) and (c), the total mass in the engine - m is calculated using the engine pressure - P, each temperature - T, each volume - V and the gas constant - R.

$$m = \frac{P\,V_E}{R\,T_E} + \frac{P\,V_R}{R\,T_R} + \frac{P\,V_C}{R\,T_C} \tag{10}$$

The temperature ratio - t, a swept volume ratio - v and other dead volume ratios are found using the following equations.

$$t = \frac{T_C}{T_E} \tag{11}$$

$$v = \frac{V_{SC}}{V_{SE}} \tag{12}$$

$$X_{DE} = \frac{V_{DE}}{V_{SE}} \tag{13}$$

$$X_{DC} = \frac{V_{DC}}{V_{SE}} \tag{14}$$

$$X_R = \frac{V_R}{V_{SE}} \tag{15}$$

The regenerator temperature - T_R is calculated in equation (16), by using the assumption (f).

$$T_R = \frac{T_E + T_C}{2} \tag{16}$$

By substituting equations (7), (8) into (10) and the total mass of the gas m is described by the following equation:

$$m = \frac{P\ V_{SE}}{2\ R\ T_C}\ [S - B\cos(x - a)] \tag{17}$$

$$a = tan^{-1}\left[\frac{v\sin(dx)}{t+\cos(dx)}\right] \tag{18}$$

$$S = t + 2tX_{DE} + \frac{4tX_R}{1+t} + v + 2X_{DC} \tag{19}$$

$$B = \sqrt{t^2 + 2tvcos(dx) + v^2} \tag{20}$$

The engine Pressure (P) is defined as the next equation

$$P = \frac{2\ m\ R\ T_C}{V_{SE}[S - Bcos(\theta - \alpha]} \tag{21}$$

The mean Pressure (P_{mean}) can be calculated as follows

$$P_{mean} = \frac{2\ m\ R\ T_C}{V_{SE}\sqrt{S^2 - B^2}} \tag{22}$$

Therefore, the engine Pressure based on the mean Pressure can be rewritten as:

$$P = \frac{P_{mean}\sqrt{1-c^2}}{1-c\ cos(x-a)} \tag{23}$$

Where the parameter c is defined as

$$c = \frac{B}{S} \tag{24}$$

Based on equation (21) it can be said that the minimum engine Pressure is when $cos(\theta - \alpha) = -1$ and the maximum when $cos(\theta - \alpha) = 1$. Therefore, the engine Pressure can be written both in terms of the minimum and maximum pressure as follows:

$$P = \frac{P_{min}\ (1+c)}{1-c\ cos(x-\alpha)} = \frac{P_{max}\ (1-c)}{1-c\ cos(x-\alpha)} \tag{25}$$

2.1.2. Beta (β) Stirling Configuration

The beta configuration features a single power piston and a displacer working inside the same cylinder. This makes it quite compact and there is typically a minimal amount of dead space as there are no interconnecting passageways. It is mechanically simple as both piston and displacer are connected at a common point on the crankshaft, with the only difficulty arising from the fact that the connecting shaft for the displacer must pass through the piston where it must make a pressure-tight seal. The purpose of the displacer is to "displace" the working gas at constant volume and shuttle it between the expansion and the compression spaces through the series arrangement cooler, regenerator, and heater. In actual engines the linkage driving the piston and displacer will move them such that the gas will compress while it is mainly in the cool compression space and expand while in the hot expansion space.

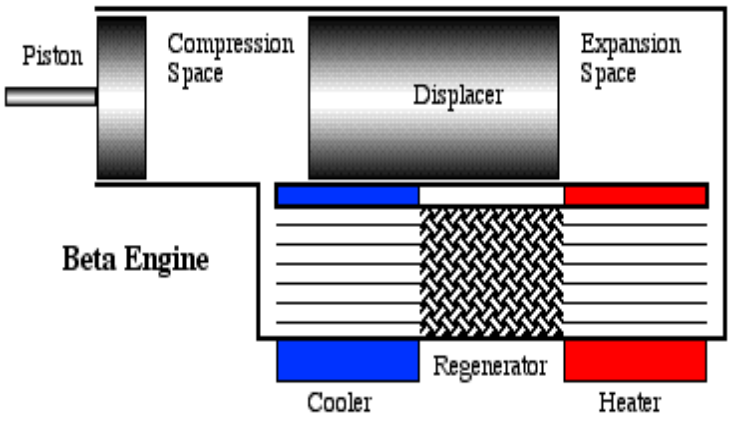

Figure 10. Beta type Stirling engine (mechanical configuration).

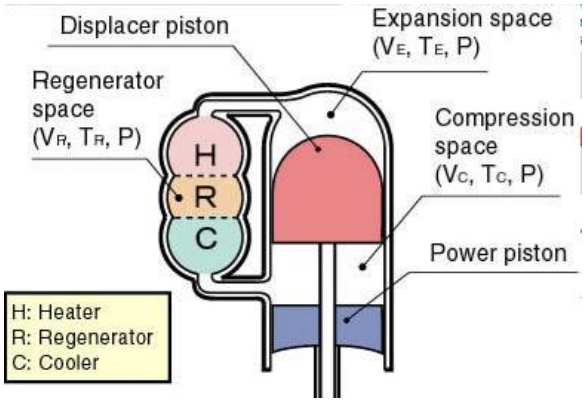

Figure 11. Schematic of beta type Stirling engine configuration.

Similarly, the equations for Beta-type Stirling engine are declared. Figure 11 shows a calculation model of a Beta-type Stirling engine. The expansion instantaneous volume V_E and the compression instantaneous volume V_C are described in the following equations, with a swept volume of a displacer piston V_{SE}, a swept volume of a power piston V_{SC} and a phase angle *dx* between the displacer piston and power piston.

$$V_E = \frac{V_{SE}}{2}(1 - cosx) + V_{DE} \tag{26}$$

$$V_C = \frac{V_{SE}}{2}(1 + cosx) + \frac{V_{SC}}{2}[1 - \cos(x - dx)] + V_{DC} - V_B \tag{27}$$

In the case of the Beta-type Stirling engine, the displacer piston and the power piston are located in the same cylinder. When both pistons overlap their stroke, an effective working space is created. The overlap volume V_B in equation (27) can be calculated in the next equation.

$$V_B = \frac{V_{SE} + V_{SC}}{2} - \sqrt{\frac{{V_{SE}}^2 + {V_{SC}}^2}{4} - \frac{V_{SE}\, V_{SC}}{2} cos(dx)} \quad (28)$$

Then the total instantaneous volume V is again as in the alpha type configuration described by equation (9)

The engine pressure is again described by equations (21) to (23).

In addition to the ratios and coefficient described above for the alpha type configuration some new ones needed here are the following:

$$X_B = \frac{V_B}{V_{SE}} \quad (29)$$

$$a = tan^{-1}\left[\frac{v \sin(dx)}{t + \cos(dx) + 1}\right] \quad (30)$$

$$S = t + 2tX_{DE} + \frac{4tX_R}{1+t} + v + 2X_{DC} + 1 - 2X_B \quad (31)$$

$$B = \sqrt{t^2 + 2(t-1)vcos(dx) + v^2 - 2t + 1} \quad (32)$$

2.1.3. Gamma (γ) Stirling Configuration

The gamma configuration is similar to that of the beta type in that it uses a piston and a displacer both directly connected to a common crankshaft. The difference is that they are not in the same cylinder, meaning that the problems of sealing the displacer rod through the piston are avoided. The downside for this is the introduction of a gas flow passageway which increases dead space in the engine. This configuration is probably the easiest to build, especially out of budget materials. It is commonly seen in LTD 'pancake' engines.

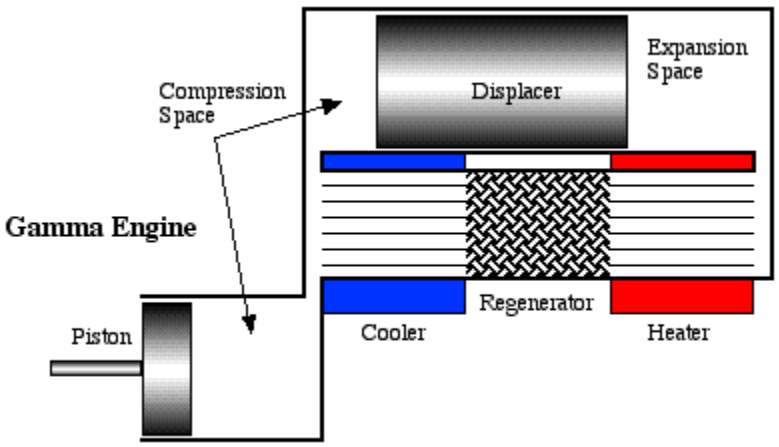

Figure 12. Gamma type Stirling engine configuration.

The equations for the instantaneous volumes and the ratios are the same as those in the Beta type configuration except for the following that are redefined as follows:

$$a = tan^{-1}\left[\frac{v\sin(dx)}{t+\cos(dx)-1}\right] \tag{33}$$

$$S = t + 2tX_{DE} + \frac{4tX_R}{1+t} + v + 2X_{DC} + 1 \tag{34}$$

$$B = \sqrt{t^2 + 2(t-1)vcos(dx) + v^2 - 2t + 1} \tag{35}$$

The indicated energy (area of the P-V diagram) in the expansion and compression space can be calculated as an analytical solution with use of the above coefficients for each type of Stirling engine configuration. The indicated energy in the expansion space (indicated expansion energy-W_E), based on the mean (P_{mean}) or either the minimum (P_{min}) or the maximum (P_{max}) pressure is described in the following equations:

$$W_E = \oint P\,dV_E = \frac{P_{mean}\,V_{SE}\,\pi\,c\,sin(\alpha)}{1+\sqrt{1-c^2}} = \frac{P_{min}\,V_{SE}\,\pi\,c\,sin(\alpha)}{1+\sqrt{1-c^2}}\cdot\frac{\sqrt{1+c}}{\sqrt{1-c}} = \frac{P_{max}\,V_{SE}\,\pi\,(1-t)\,sin(\alpha)}{1+\sqrt{1-c^2}}\cdot\frac{\sqrt{1+c}}{\sqrt{1-c}} \tag{36}$$

The indicated energy in the compression space (indicated compression energy-W_C) is:

$$W_C = \oint P\,dV_E = -\frac{P_{mean}\,V_{SE}\,\pi\,c\,t\,sin(\alpha)}{1+\sqrt{1-c^2}} = \frac{P_{min}\,V_{SE}\,\pi\,c\,t\,sin(\alpha)}{1+\sqrt{1-c^2}}\cdot\frac{\sqrt{1+c}}{\sqrt{1-c}} = \frac{P_{max}\,V_{SE}\,\pi\,c\,t\,sin(\alpha)}{1+\sqrt{1-c^2}}\cdot\frac{\sqrt{1+c}}{\sqrt{1-c}} \tag{37}$$

The indicated energy per one cycle of the engine W_i (J) is the algebraic sum of the above energies and is:

$$W_i = W_E + W_C = \frac{P_{mean}\, V_{SE}\, \pi\, c\, (1-t)\, sin(\alpha)}{1+\sqrt{1-c^2}} = \frac{P_{min}\, V_{SE}\, \pi\, c\, (1-t)\, sin(\alpha)}{1+\sqrt{1-c^2}} \cdot \frac{\sqrt{1+c}}{\sqrt{1-c}} = \frac{P_{max}\, V_{SE}\, \pi\, c\, (1-t)\, sin(\alpha)}{1+\sqrt{1-c^2}} \cdot \frac{\sqrt{1+c}}{\sqrt{1-c}} \quad (38)$$

Relations between P_{mean}, P_{min} and P_{max} are determined in the following equations:

$$\frac{P_{min}}{P_{mean}} = \sqrt{\frac{1-c}{1+c}} \quad (39)$$

$$\frac{P_{max}}{P_{max}} = \sqrt{\frac{1+c}{1-c}} \quad (40)$$

The indicated expansion power (L_E) the indicated compression power (L_C) and the indicated power of this engine (L_i) given in Watts are defined in the following equations, using the engine speed n (rps).

$$L_C = n \cdot W_C \quad (41)$$

$$L_E = n \cdot W_E \quad (42)$$

$$L_i = n \cdot W_i \quad (43)$$

The indicated expansion energy W_E found equation (36) means an input heat from a heat source to the engine while the indicated compression energy (W_C) calculated by equation (37) means a reject heat from the engine to cooling water or air. Then the thermal efficiency of the engine η is calculated in the next equation.

$$\eta_{th} = 1 - t = 1 - \frac{T_C}{T_E} \quad (44)$$

This efficiency equals that of a Cαrnot cycle that is the highest efficiency in every thermal engine.

2.2. Features of Kinetic Stirling Engines

Many different kinetic drive mechanisms have been adopted to control the movements of the mechanical pistons in Stirling engines, including the crank-slider, Ringbom, rhombic, swash-plate, and Ross-yoke drives, etc. The crank-slider drive mechanism is the most common drive for Stirling engines. The rhombic drive is typically used in single cylinder beta-type Stirling engines working at high pressures. The swash-plate drive is mainly adopted for four-cylinder double-acting Stirling engines for automobiles. The Ross-yoke drive is mostly used in small Stirling engines. Most of the previous LTD Stirling engines are the crank-slider drive gamma type, having a large and short displacer and a much smaller power piston. Some LTD Stirling engines only have the power piston linked to the crankshaft, while the displacer moves freely in response to the pressure difference between the inside of the engine and the atmosphere. This is also known as the LTD Ringbom Stirling engine. The Ross-yoke drive has been applied in some moderate temperature Stirling engines. However, no Stirling engines for low and medium temperature heat sources have ever been developed using Rhombic or swash-plate drives due to the complexity of the mechanical structures.

The main features of kinetic Stirling engines are:

i. Kinetic Stirling engines operating at high pressures need lubrication for moving components and special seals for pistons and rods to prevent gas leakage and oil pollution.
ii. The linear reciprocating motions of pistons are all converted into rotation motions using different kinds of kinetic drives.
iii. The phase difference of the power piston and displacer are mechanically fixed by the kinetic drive.
iv. The displacements of pistons are fixed at any working conditions due to the constraints of mechanical linkages. Swash-plate drive Stirling engine with a variable plate angle is an exception.
v. The only way of adjusting power output of most kinetic Stirling engines except the swash-plate one is to vary the rotating speed.
vi. An initial excitation should be provided to start kinetic Stirling engines if the heating temperature is sufficient high.

2.3. Solar – driven LTD Stirling Engine

The low temperature operating capability of the LTD Stirling engine makes it a good alternative for low-temperature solar power applications. Several concept design and numerical works have been conducted on solar-powered LTD Stirling engines since 2005. In the review paper of Thombare and Verma (Thombare DG. Verma SK., 2008) about the technological development in Stirling cycle engines, it was noted that solar-powered double-acting LTD Stirling engines working at relatively low temperatures with helium as the working fluid were potentially attractive engines for the future. Abdullah et al. (Abdullah S. Yousif BF. Sopian K., 2005),presented the design considerations for a four-cylinder double-acting Stirling engine for solar applications at the heating temperature of 70 C. Shazly et al. (Shazly JH. Hafez AZ. El Shenawy ET. Eteiba MB., 2014), carried out a thermal analysis of a small solar-powered LTD Stirling engine based on a heat transfer model and the Beale formula. Kerdchang et al. (Kerdchang P. MaungWin M. Teekasap S. Hirunlabh J. Khedari J. Zeghmati B., 2005) conducted a conceptual design and numerical study of a Beta-type Stirling solar engine for circulating water applications for ventilation. The unique features of the design were that R-11 was used as working fluid and check valves were employed for controlling the flow direction of fluid. More experimental solar-powered LTD Stirling engines were constructed and investigated.

Tavakolpour et al. (Tavakolpour AR. Zomorodian A. Golneshan AA., 2008) built and tested a solar-powered LTD Stirling engine with two cylinders connected on one shaft. A flat-plate solar collector which reached a heating temperature of around 100^{o}C to 278^{o}C was employed as the in-built heat source. A finite heat transfer model was first used to calculate the gas temperatures in the hot and cold spaces. Classical Schmidt theory was then employed to evaluate the theoretical output work and optimize phase angle according the obtained temperatures. It was indicated that the thermal efficiency can be effectively increased if the regenerator effectiveness is increased from zero to one. Experiments were then conducted on the engine without a regenerator, i.e. annual gap between displacer and cylinder as the regenerative passage. A maximum power of 0.27 W was reported on the engine operating at 14 rpm with a collector temperature of 110 ◦C and sink temperature of 25C.

In the past ten years, Kongtragool and Wongwises conducted a series of work on LTD Stirling engines for solar energy utilizations. In 2007, a twin power piston LTD Stirling engine was built (Kongtragool B., 2007). It had two power pistons with a total swept volume of 893 cm3, and one displacer with swept volume of 6,394 cm^3. The displacer also functioned as a moving regenerator which used stainless steel pot sourer as the regenerative matrix. The performance of the engine with ambient air as the working gas was first tested with a tungsten halogen lamp as the solar simulator. Maximum output powers ranged from 0.88 W to 1.69 W when the heating temperature was within the range of 126^{o}C - 163^{o}C. The corresponding thermal efficiencies and speeds were around 0.5% and 50 rpm, respectively. When the engine was powered by a LPG burner, a maximum shaft power of 11.8 W at 133 rpm was achieved at 316^{o}C. However, the heat source was a solar simulator made from a 1000 W halogen lamp.

Comparisons were made between the characteristics of the high-temperature differential (HTD) and LTD Stirling engine and methods for performance improvement were also discussed. Although some information is currently available on the LTD Stirling engine, there still remains room for further research. In particular, a detailed investigation is lacking into the LTD Stirling engine using solar energy as a heat source.

Robson (Robson AP., 2007) developed a LTD Ringbom Stirling engine based on a third order numerical analysis method. The experimental engine had a swept volume of 16 cm^3 and four regenerators embedded inside the displacer. It started to run at a temperature difference of 62^{o}C. The engine speed ranged around 200-220 rpm when the temperature difference was in the region of 80^{o}C.

Kongtragool and Wongwises (Kongtragool B. Wongwises S., A four power-piston low-temperature differential Stirling engine using simulated solar energy as a heat source, 2008) presented a kinematic, single-acting, four power-piston, gamma configuration LTD Stirling engine that was tested with a solar simulator using non-pressurized air as a working fluid. Four 1000 W halogen lamps were used in the solar simulator. The engine was tested with four different simulated solar intensities. Results from this study indicate that the engine performance and heater temperature increase with increasing simulated solar intensity. In fact, findings indicate that the maximum engine torque, shaft power, and brake thermal efficiency increases with increasing heater temperature. At the maximum simulated solar intensity of 7094W/m2, or actual heat input of 1378 W

and a heater temperature of 439 K, the engine produces a maximum torque of 2.91 Nm, a maximum shaft power of 6.1 W, and a maximum brake thermal efficiency of 0.44% at 20 rpm, approximately.

In 2008, they also constructed and tested a small single piston LTD Stirling engine driven by actual solar energy by using a parabolic-dish concentrator (Kongtragool B. Wongwises S., Testing of a low-temperature differential Stirling engine by using actual solar energy , 2008). A small DC generator was connected to the engine to generate electricity. A maximum electric power of 2.3 W with an overall efficiency of around 0.1% was reported.

Cinar et al. (Cinar C. Aksoy F. Erol D., 2012) investigated the effect of displacer material on the performance of a LTD Stirling engine. The engine was tested with two different displacers made of aluminium alloy and medium density fibreboard. The results indicated that the engine with the displacer made of medium density fibreboard had a better performance in the aspects of power output and torque. It started to run at the heating temperature of 235^{o}C with aluminium alloy displacer and only 115^{o}C with the medium density fibreboard displacer. The highest power provided by the medium density fibreboard displacer was 3.06W at 160^{o}C, while the power achieved by the aluminium alloy displacer was 2.59 W at 320^{o}C. The performance improvement was because of the lower thermal conductivity and lower density of the non-metallic displacer.

Iwamoto et al. (Gentherm, n.d.), (Iwamoto I. Toda F. Hirata K. Takeuchi M. Yamamoto T., 1997) built a 300 W class LTD Stirling engine. A maximum output power of about 146 W was reported at a rotating speed of about 143 rpm when the heat source temperature was130^{o}C. The indicated efficiency achieved 5% when it operated at the maximum output power. It reached approximately 50% of the Carnot efficiency at its rated speed. Later, they developed an even larger LTD Stirling engine at the power range of 1 kW. It was an alpha-type engine with two power pistons coaxially arranged. The diameter of the cylinder was 400 mm and the total weight of the engine was up to 2 tons. According to the reported data, it reached nearly 700 W under a temperature difference of only 80 C (Kolin I. Koscak-Kolin S. Golub M., 2000). Their results showed that it is technically possible for LTD Stirling engines to be scaled up to have power outputs of practical uses.

Many companies have also shown their interests in developing large scale LTD Stirling engines up to hundreds to kilowatts for utilizing geothermal energy, solar energy, low grade industrial waste heat, etc. However, few scientific literatures about the design and performances have been disclosed probably due to the commercial considerations.

2.4. Moderate Temperature Kinetic Stirling Engine

Moderate solar concentration to temperature levels of 250°C to 450°C may be of interest for power generations using solar-Stirling systems with lower costs compared to those of high temperature solar concentrations. Different from the low-cost LTD Stirling engines that do not have regenerators and use ambient air as working gas, most of the moderate temperature Stirling engines have regenerators made of porous media and use pressured gas as working fluid to get better performances. The effects of regenerator types and materials on the performances have been intensively investigated for moderate temperature Stirling engines.

In 2008, Isshiki et al. (Isshiki S. Sato H. Konno S. Shiraishi H. Isshiki N. Fujii I., 2008) experimentally studied and compared the performances of a beta-type Stirling engine using layered-plate type and stainless wire-mesh type regenerators. The results indicated that the layered-plate type regenerator showed better performance compared to the wire-mesh one. It was explained that the flow resistance through layered-plate was much smaller because the flow through layered-plate was laminar while that through the wire-mesh became middle region of laminar flow and turbulent flow. The enlarged heat transfer area of layered-plate compared to that of the wire-mesh was considered to be the other reason. The achieved shaft power ranged from about 22 W to 91.4 W when the temperature difference was in the range of 180°C to 330°C.

Karabulut et al. (Karabulut H. Cinar C. Ozturk E. Yucesu HS., 2010) designed and manufactured a beta-type Stirling engine with a displacer driven by a novel lever mechanism, as shown in Figure 4. The engine was aimed for low and moderate temperature energy sources at the ranges of 200°C to 500°C. Two different displacer cylinders, including the one with a smooth inner surface and the other one with rectangular slots augmented inner surface, were tested and compared as the regenerative channels. The results showed that the engine with the slotted cylinder provided about 50% higher power than that of the smooth cylinder due to the enlarged heat transfer area. Maximum power output was obtained as about 52 W at 453 rpm when it worked at 200C with 2.8 bar air (Karabulut H, 2009). The thermal efficiency reached as high as 15%, corresponding to 41% of the Carnot efficiency. When the engine was charged with helium, the minimum heating temperature for the engine to run was

measured to be 118°C (Karabulut H, 2009). The maximum power was measured as 183W at 4 bar charge pressure and 260°C heating temperature. It was reported that the motion of the displacer governed by the lever mechanism was able to have a better approach to theoretical Stirling cycle. Comparisons with the crank-drive and Rhombic-drive engines based on thermodynamic analysis indicated that the lever-drive engine has the highest work per cycle at the same charge pressure (Karabulut H. Aksoy F. Ozturk E., 2009).

Chen et al. (Chen WL. Wong KL. Po LW., 2012), built a prototype helium charged twin power piston gamma-type Stirling engine. Annular gas between the displacer and its cylinder was first adopted as the regenerative channel for the prototype engine. A numerical investigation showed that the regeneration effectiveness posed crucial impact on the engine's performance. Running the prototype engine at a heating temperature of 200°C gave a power output of 3.6W at a speed of 104 rpm in the experiment. Later, they modified the displacer into a moving regenerator, and carried out experimental studies on effects of several regenerator parameters on the overall performances (Chen WL. Wong KL. Chen HE., 2014). It was found the copper stacked-woven screen was a superior regenerator material than the stainless steel one for their Stirling engine. They pointed out that how the regenerator matrices were placed relatively to the direction of gas flow was an important factor affecting the overall performance. Better performance was found when the screens were installed perpendicular to the screen surfaces. The output power of the engine ranged from about 10 W to 100 W at the heating temperature range of 200°C to 400°C. The efficiency ranged approximately from 1% to 10%.

Recently, they developed a three-dimensional compressible computational fluid dynamics code to study the heat transfer characteristics of the twin power piston Stirling engine (Chen WL. Wong KL. Chang YF., 2014). It was found that the impingement was the dominant heat transfer mechanism in the expansion and compression spaces, and temperature distribution across the engine volume at any moment was highly non-uniform. Their results showed that the heat transfer was so complex that the treatment of constant heat transfer coefficients by some zero- or one-dimensional models was inadequate to reflect the reality Gheith et al. (Gheith R. Aloui F. Nasrallah SB., 2015) experimentally studied the performances of an air-charged gamma type Stirling engine with different regenerator materials. The piston and the displacer were connected to a

shaft with a phase difference of 90 degrees. Performances of the engine with four different materials including stainless steel, copper, aluminium, and Monel 400 were characterized. The stainless steel was proved to be the best regenerator material in consideration of the performance and the problem of oxidation. By optimizing the porosity of the stainless-steel regenerator, the engine produced brake powers of 200 W-300 W at the heating temperatures of 300°C to 500°C. The maximum relative Carnot efficiency reached more than 20% at 300°C.

Sripakagorn and Srikam (Sripakagorn A. Srikam C., 2011) designed and experimentally investigated a prototype beta type Stirling engine aiming for concentrating solar power generation. The heating temperature was designed between 350°C and 500°C, which is the typical temperature range available from the parabolic trough solar collector. The displacer was designed to have a length to diameter ratio of 1.35, which was between the typical values of LTD Stirling engines (less than unity) and the high temperature ones. Stainless steel mesh was filled in the annual regenerator as the regenerative material. The engine was tested to have a maximum power of 26.6 W and a highest efficiency of about 5.5% with 7 bar air at the heating temperature of 350°C. When the heating temperature was increased to 500°C, the maximum output power and efficiency reached 95.4 W and 9.35%, respectively. Their comparisons of the dimensionless West numbers and the specific powers of previous prototypes showed that the developed moderate temperature Stirling engine had a comparable specific power over some of the high temperature ones with simpler and less costly development.

2.5. Simple Theoretical Analysis of Stirling Engines

The simplest analysis is that for the ideal Stirling cycle, where the thermodynamic cycle comprises two isothermal and two constant volume regenerative processes. However, this involves such gross idealization of the process occurring in an actual Stirling engine as to a suitable only for the most elementary, preliminary design calculations.

A more realistic analysis was devised by Gustav Schmidt (1871). His analysis has become a classical one and gives a more reasonable approximation of the engine performance although it still remains highly idealized. The real performance of an engine would be approximately no better than 60% of the predicted Schmidt cycle performance and often even less. The reason behind this is that the processes of compression and expansion in the engine cylinders are more nearly adiabatic than isothermal causing a redistribution of the cylinder mass variation of the working fluid and consequently, on the performance of the engine.

Principal Assumptions of Schmidt Theory

a. There is no pressure loss in the heat exchangers and there are no internal pressure differences, thus the pressure is constant throughout the system.
b. The expansion process and the compression process are isothermals.
c. The working fluid obeys the characteristic gas equation: PV = m RT.
d. The speed of the engine is constant.
e. The regenerative process is perfect.
f. The volume variations in the working space occur sinusoidal.
g. There are no temperature gradients in the heat exchangers.
h. The cylinder-wall piston temperatures are constant.
i. There is no leakage, and the mass of the working fluid remains constant.
j. The expansion dead space maintains the expansion gas temperature (T_E) and the compression dead space maintains the compression gas temperature (T_C) during the cycle.
k. The regenerator gas temperature is an average of the expansion gas temperature - T_E and the compression gas temperature - T_C.

Finkelstein (1961) nearly a century ago after Schmidt analysis derived a generalized analysis in which the processes of compression and expansion in the cylinders could be specified to occur between the two limiting cases:

(a) isothermal (infinite rates of heat transfer between the working gas and the cylinder walls)
(b) adiabatic (zero rates of heat transfer between the working gas and the cylinder walls)

The model assumed that, in the heater and cooler, infinite heat transfer and isothermal conditions prevailed so that fluid in the heat exchangers was always at the upper temperature T_E or the lower temperature T_C. The temperature of the working fluid in the cylinders varied during the cycle and could be greater or less than T_E (in the expansion space) or T_C (in the compression space). Finkelstein's generalized analysis retained all the other significant assumptions enumerated in the Schmidt cycle and therefore it still remained highly idealized. Nevertheless, the possibility for non-isothermal processes represented the new theoretical development by that time.

Later Khan (1962) investigated the effect of variations in the principal design parameters and obtained numerical results for a large number of different cases with adiabatic compression and expansion processes, some of those were summarized by Walker and Khan (1965). In these models the thermal efficiency became a function, not only of the temperature (as in the isothermal cycle) but also of the swept volume ratio, the phase angle and the dead volume ratio. An unexpected result based on this theory was that with the increase in the dead space of the engine the thermal efficiency increased even though the power output declined (as predicted in the Schmidt theory).

Significant work using the adiabatic cycle approach was reported by Qvale and Smith (1969) and by Rios and Smith (1969). They consider a basic cycle with adiabatic compression and expansion separately assess the effects of irreversibility. This approach allows for independent study of individual heat exchange components in a series of successive approximations that can be extended to the required degree of complexity.

Chapter 3

Calculation Results

2.1. Effect of the temperature difference

In this chapter, a study is carried out on the effect of the temperature difference on the three types of mechanical configuration of an ideal Stirling engine (based on the assumption of the isothermal compression and expansion).

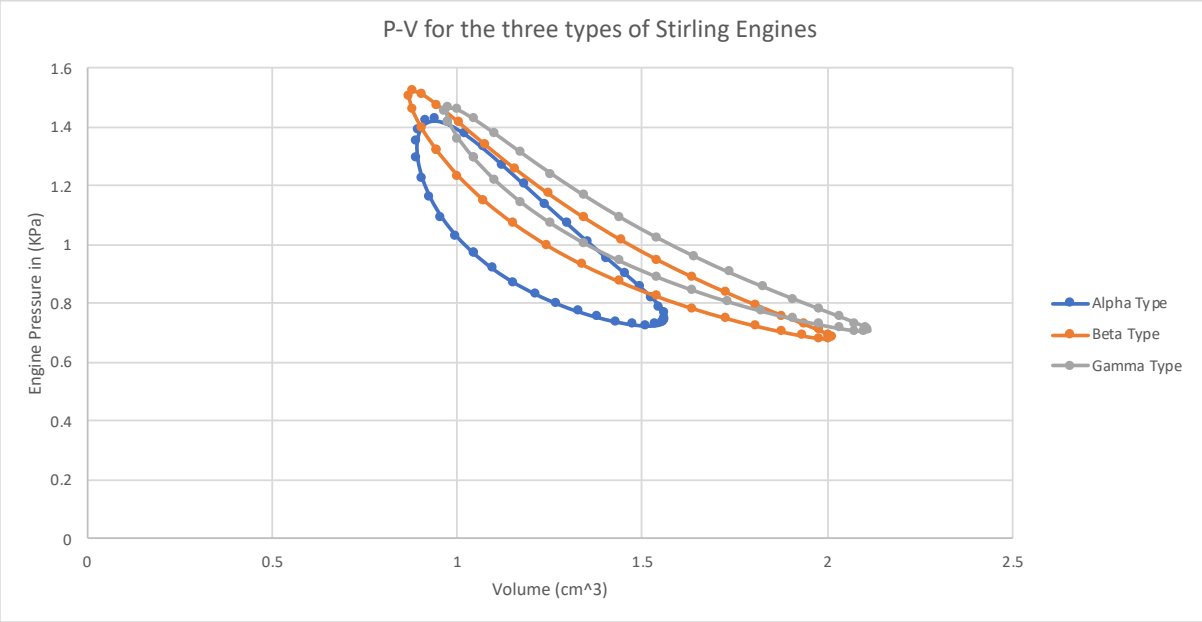

Figure 13. P-V diagram of all three (α, β, γ-type Stirling Engine configurations) for Tcold =30oC Thot=400oC and 115 degrees phase angle.

Table 1. Comparison between the Indicated Energies and Power for all the three types of Stirling Engine configurations for Tcold =30oC Thot=400oC and 115 degrees phase angle.

	Alpha Type Stirling	Beta Type Stirling Engine	Gamma Type Stirling
Indicated Expansion Energy WE (J)=	0,033637293	0,02644499	0,024088786
Indicated Compression Energy WC (J)=	-0,015144279	-0,01190614	-0,010845323
Indicated Energy per one cycle Wi(J)=	0,018493014	0,014538851	0,013243463
Indicated Power of Engine Li(W)=	0,616433804	0,484628354	0,441448773

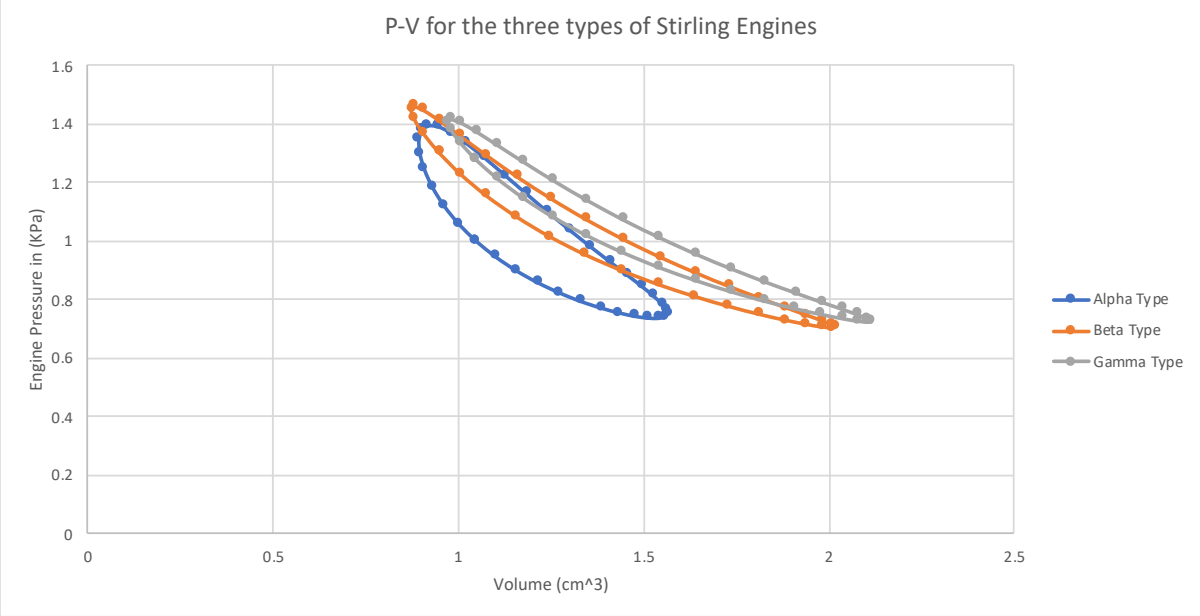

Figure 14. : P-V diagram of all three (α, β, γ-type Stirling Engine configurations) for Tcold =30oC Thot=300oC and 115 degrees phase angle.

Table 2. Comparison between the Indicated Energies and Power for all the three types of Stirling Engine configurations for Tcold =30oC Thot=300oC and 115 degrees phase angle.

	Alpha Type	Beta Type Stirling	Gamma Type

	Stirling	Engine	Stirling
Indicated Expansion Energy WE (J)=	0,031556586	0,022942097	0,021011644
Indicated Compression Energy WC (J)=	-0,01668699	-0,012131685	-0,01111087
Indicated Energy per one cycle Wi(J)=	0,014869595	0,010810412	0,009900775
Indicated Power of Engine Li(W)=	0,49565318	0,360347075	0,330025829

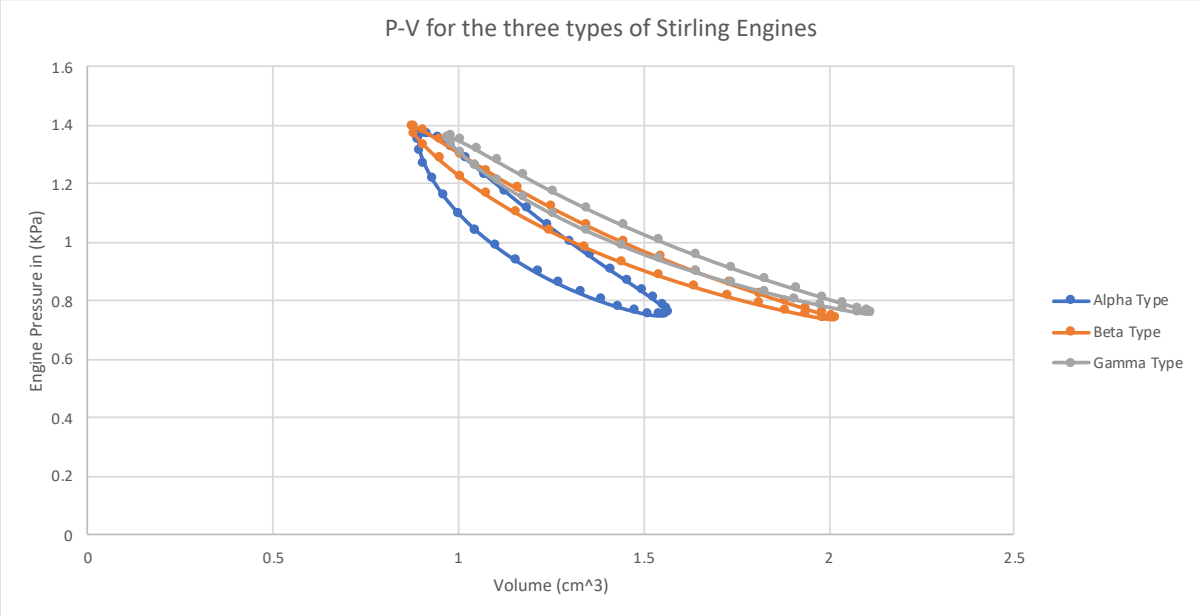

Figure 15. P-V diagram of all three (α, β, γ-type Stirling Engine configurations) for Tcold =30oC Thot=200oC and 115 degrees phase angle.

Table 3. Comparison between the Indicated Energies and Power for all the three types of Stirling Engine configurations for Tcold =30oC Thot=200oC and 115 degrees phase angle.

	Alpha Type Stirling	Beta Type Stirling Engine	Gamma Type Stirling
Indicated Expansion Energy WE (J)=	0,029098253	0,018922052	0,017440592

Indicated Compression Energy WC (J)=	-0,018640107	-0,012121314	-0,011172303
Indicated Energy per one cycle Wi(J)=	0,010458146	0,006800737	0,006268289
Indicated Power of Engine Li(W)=	0,348604869	0,226691246	0,208942959

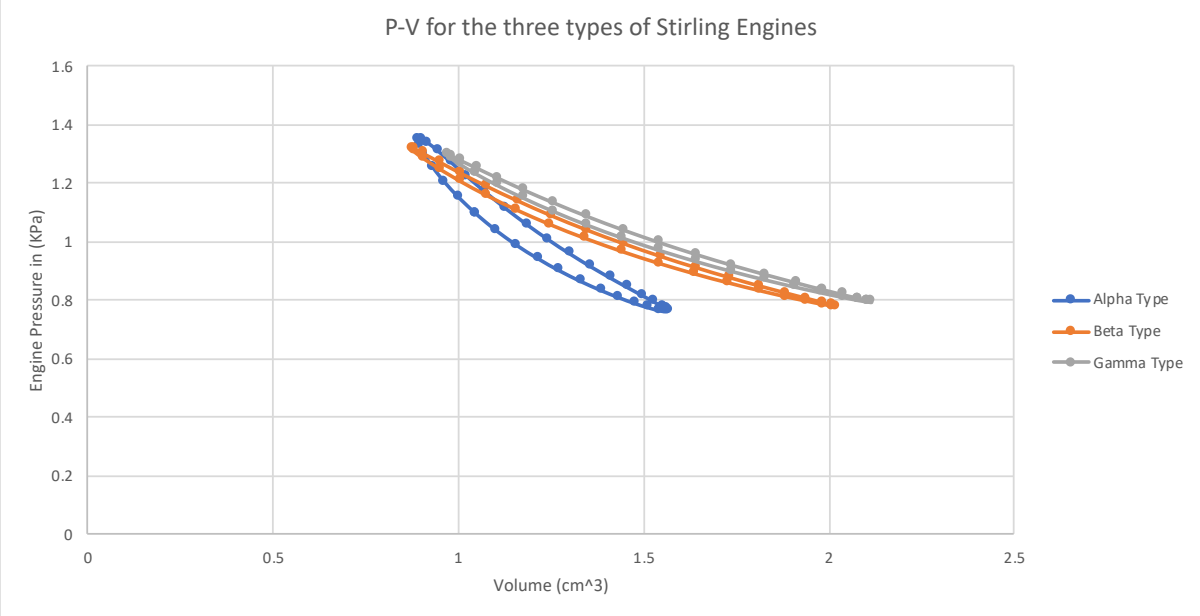

Figure 16. P-V diagram of all three (α, β, γ-type Stirling Engine configurations) for Tcold =30oC Thot=100oC and 115 degrees phase angle.

Table 4. Comparison between the Indicated Energies and Power for all the three types of Stirling Engine configurations for Tcold =30oC Thot=100oC and 115 degrees phase angle.

	Alpha Type Stirling	**Beta Type Stirling Engine**	**Gamma Type Stirling**
Indicated Expansion Energy WE (J)=	0,026124941	0,014366398	0,013343493
Indicated Compression Energy WC (J)=	-0,021222137	-0,011670291	-0,010839353
Indicated Energy per one	0,004902804	0,002696107	0,002504141

cycle Wi(J)=			
Indicated Power of Engine Li(W)=	0,163426798	0,089870231	0,083471362

2.2. Effect of the phase angle

In this chapter, a study is carried out on the effect of the phase angle on the three types of mechanical configuration of an ideal Stirling engine (based on the assumption of the isothermal compression and expansion)

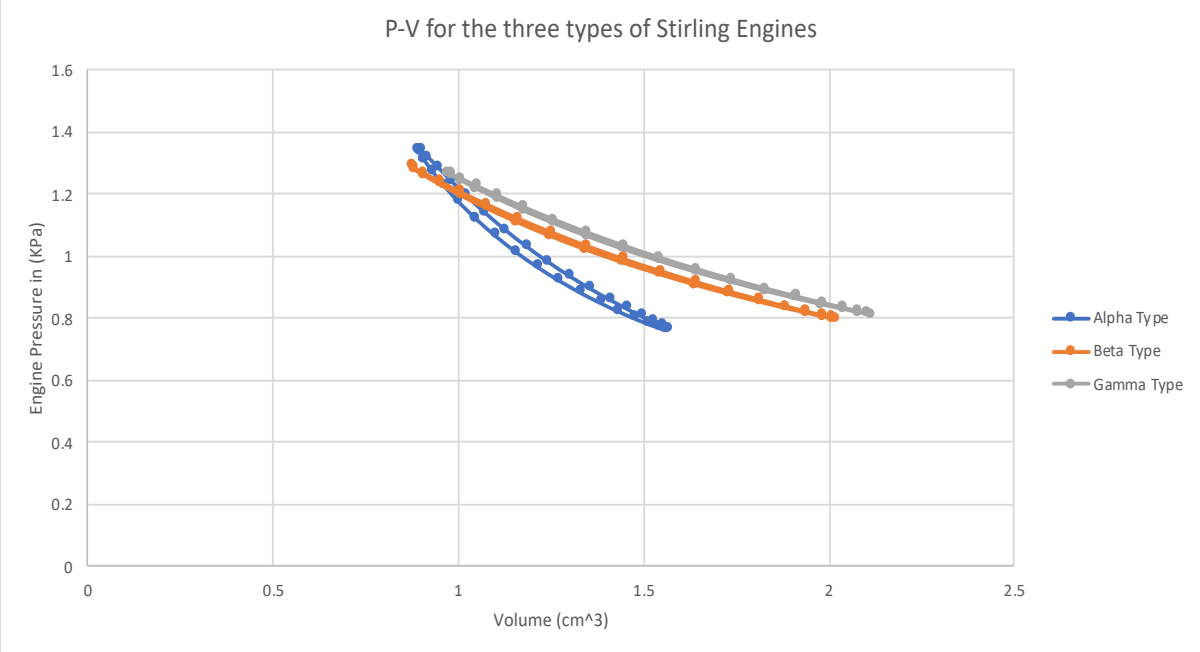

Figure 17. P-V diagram of all three (α, β, γ-type Stirling Engine configurations) for Tcold =30oC Thot=60oC and 115 degrees phase angle.

Table 5. Comparison between the Indicated Energies and Power for all the three types of Stirling Engine configurations for Tcold =30oC Thot=60oC and 115 degrees phase angle.

	Alpha Type Stirling	Beta Type Stirling Engine	Gamma Type Stirling
Indicated Expansion Energy WE (J)=	0,024744089	0,012427842	0,011584031
Indicated Compression Energy WC (J)=	-0,022514892	-0,011308217	-0,010540424
Indicated Energy per one cycle Wi(J)=	0,002229197	0,001119625	0,001043606
Indicated Power of Engine Li(W)=	0,074306573	0,037320847	0,034786879

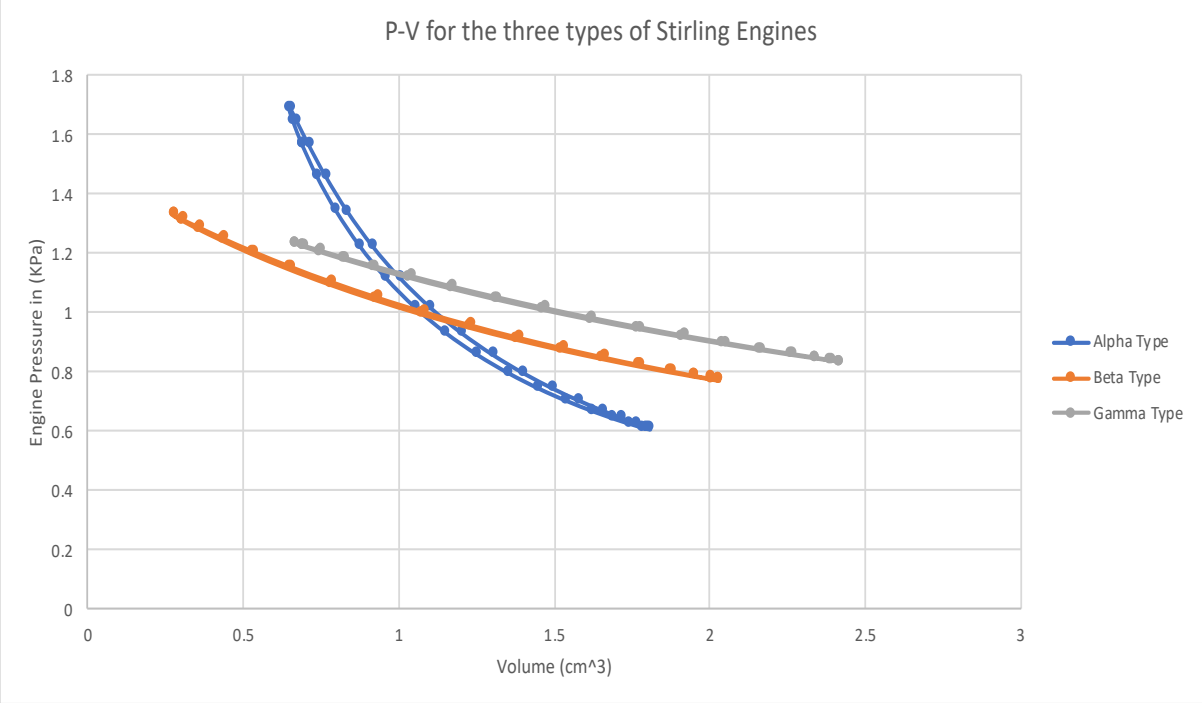

Figure 18. P-V diagram of all three (α, β, γ-type Stirling Engine configurations) for Tcold =30oC Thot=100oC and 45 degrees phase angle.

Table 6. Comparison between the Indicated Energies and Power for all the three types of Stirling Engine configurations for Tcold =30oC Thot=100oC and 45 degrees phase angle.

	Alpha Type Stirling	Beta Type Stirling Engine	Gamma Type Stirling
Indicated Expansion Energy WE (J)=	0,021246214	0,007305753	0,005272188
Indicated Compression Energy WC (J)=	-0,017258989	-0,0059347	-0,004282769
Indicated Energy per one cycle Wi(J)=	0,003987225	0,001371053	0,000989419
Indicated Power of Engine Li(W)=	0,132907505	0,04570176	0,032980621

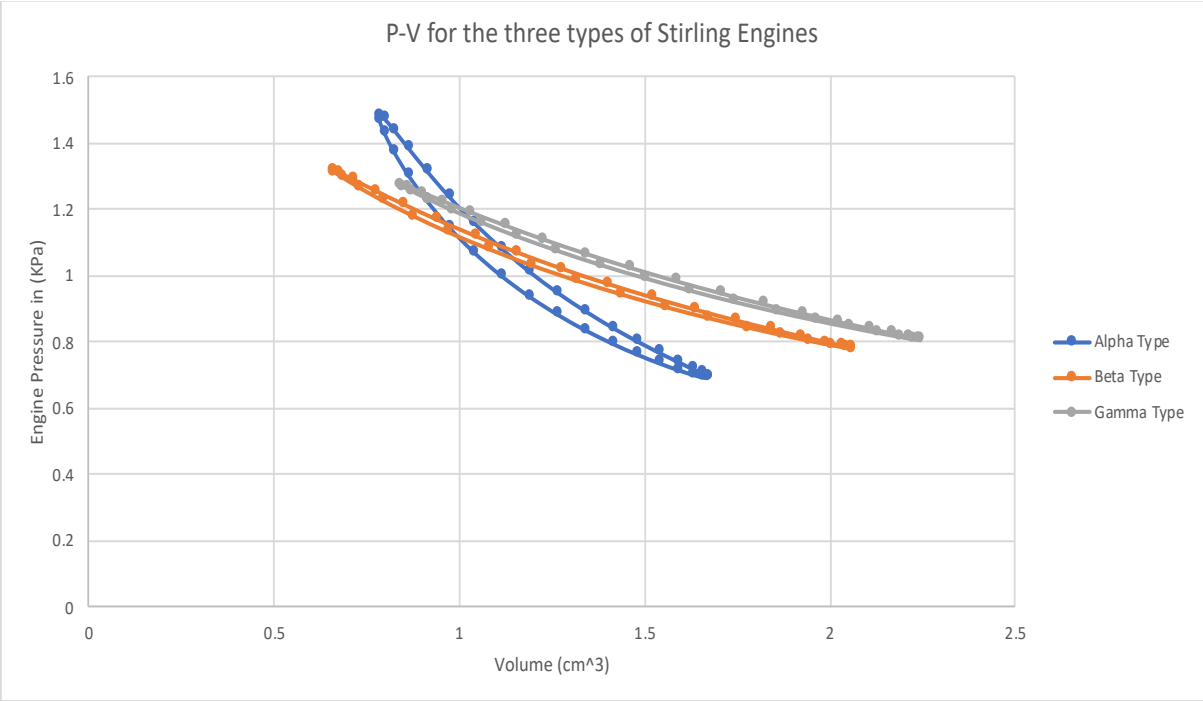

Figure 19. P-V diagram of all three (α, β, γ-type Stirling Engine configurations) for Tcold =30oC Thot=100oC and 90 degrees phase angle.

Table 7. Comparison between the Indicated Energies and Power for all the three types of Stirling Engine configurations for Tcold =30oC Thot=100oC and 90 degrees phase angle.

	Alpha Type Stirling	Beta Type Stirling Engine	Gamma Type Stirling
Indicated Expansion Energy WE (J)=	0,029258554	0,012645563	0,010967087
Indicated Compression Energy WC (J)=	-0,023767673	-0,010272401	-0,008908921
Indicated Energy per one cycle Wi(J)=	0,005490881	0,002373162	0,002058166
Indicated Power of Engine Li(W)=	0,183029383	0,079105397	0,068605549

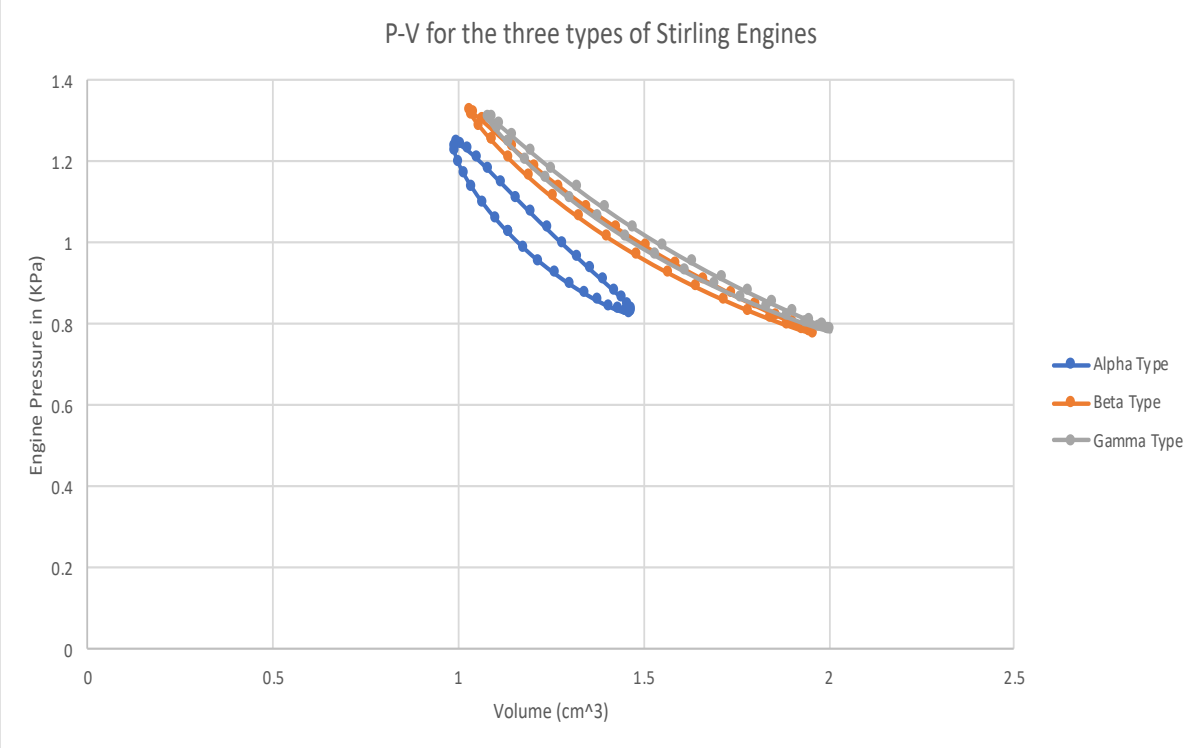

Figure 20. P-V diagram of all three (α, β, γ-type Stirling Engine configurations) for Tcold =30oC Thot=100oC and 135 degrees phase angle.

Table 8. Comparison between the Indicated Energies and Power for all the three types of Stirling Engine configurations for Tcold =30oC Thot=100oC and 135 degrees phase angle.

	Alpha Type Stirling	Beta Type Stirling Engine	Gamma Type Stirling
Indicated Expansion Energy WE (J)=	0,020186772	0,01425358	0,013759212
Indicated Compression Energy WC (J)=	-0,01639837	-0,011578645	-0,011177054
Indicated Energy per one cycle Wi(J)=	0,003788402	0,002674935	0,002582158
Indicated Power of Engine Li(W)=	0,126280076	0,089164484	0,086071926

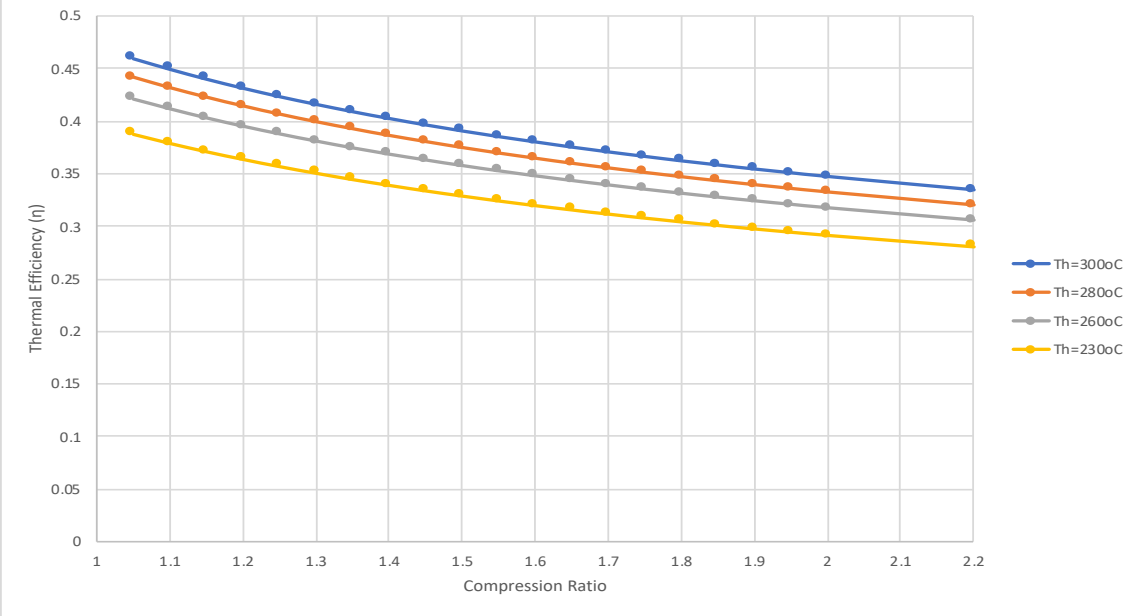

Figure 21. Thermal efficiency versus compression ratio for ideal Schmidt cycle (isothermal compression & expansion) for a range of temperatures for the hot medium [230-300 degrees].

Table 9. Efficiency results for both Carnot and Carlquist for Th between 503 and 573.

Tc (K)=	**303**							
Th (K)=	573	563	553	543	533	523	513	503
Th-Tc (oC or K)=	270	260	250	240	230	220	210	200
η Carnot	0,471204	0,46181	0,45207	0,44198	0,4315	0,4206	0,40935	0,39761
ηCarlquist	0,241256	0,23644	0,23146	0,22629	0,22093	0,21537	0,20959	0,20357

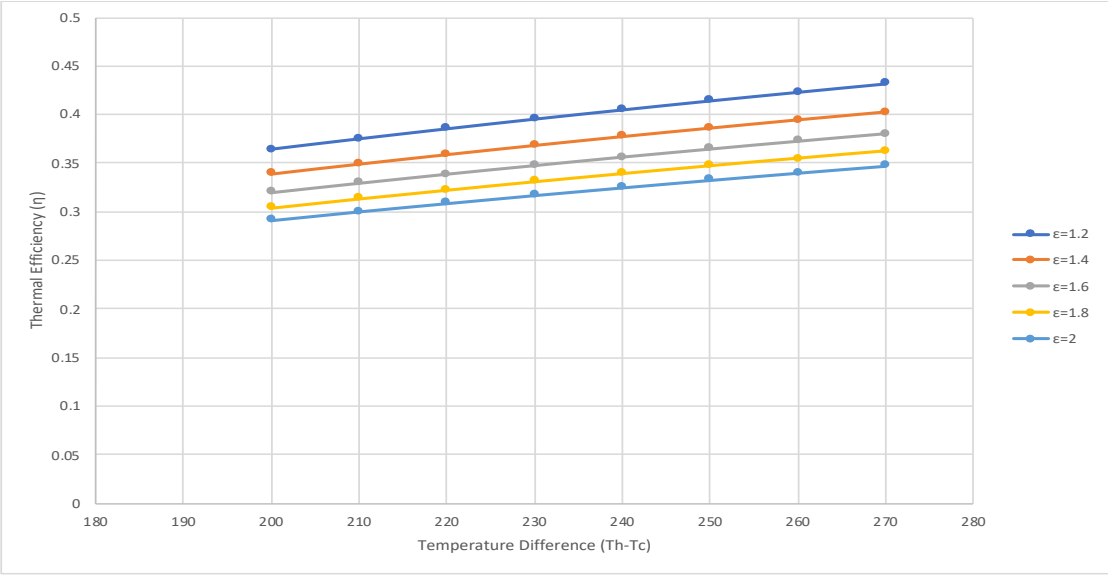

Figure 22. Thermal efficiency versus Temperature difference between hot and cold medium for ideal Schmidt cycle (isothermal compression & expansion) for different compression ratios.

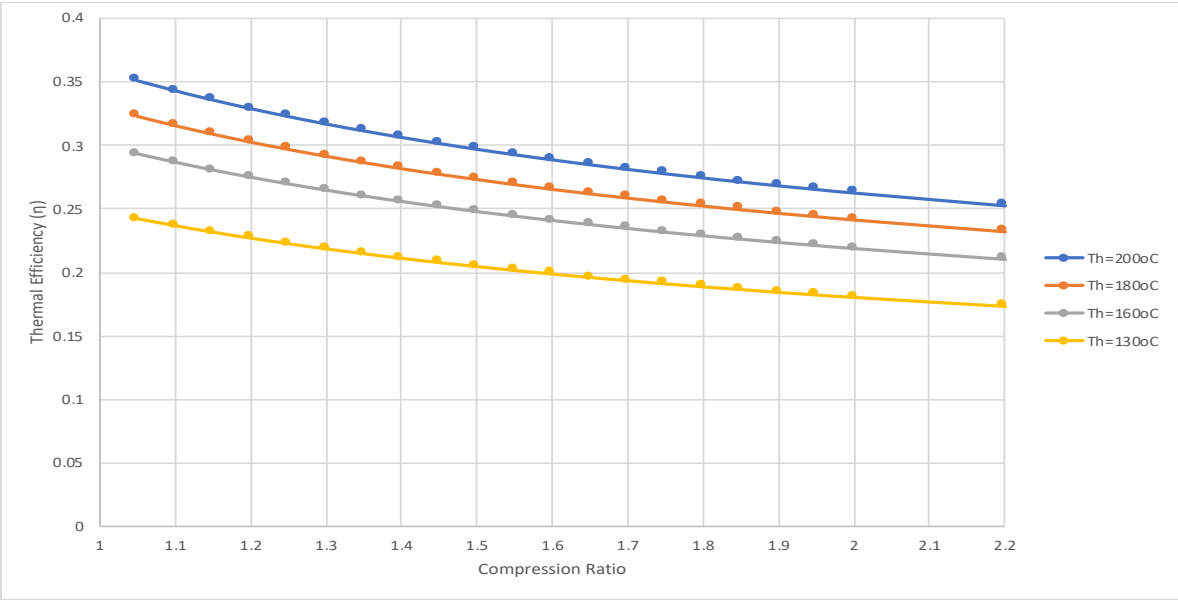

Figure 23. Thermal efficiency versus compression ratio for ideal Schmidt cycle (isothermal compression & expansion) for a range of temperatures for the hot medium [130-200 degrees].

Table 10. Efficiency results for both Carnot and Carlquist for Th between 403 and 473.

Tc (K)= 303

Th (K)=	473	463	453	443	433	423	413	403
Th-Tc (oC or K)=	170	160	150	140	130	120	110	100
η Carnot	0,359408	0,345572	0,33112	0,31602	0,30023	0,28368	0,26634	0,24813
ηCarlquist	0,184016	0,17693	0,16953	0,16180	0,15371	0,14524	0,13636	0,12704

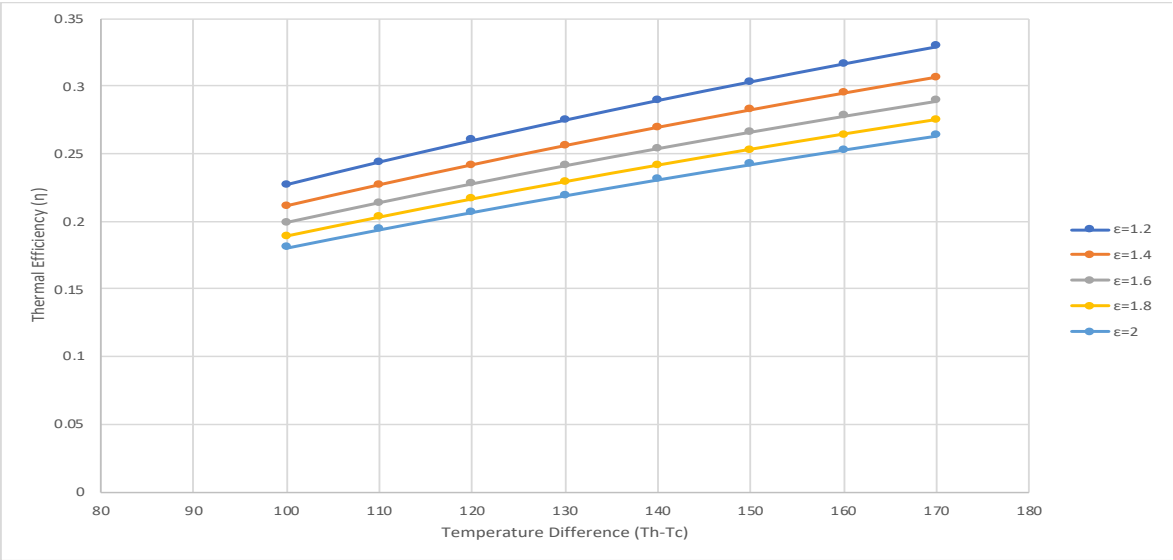

Figure 24. Thermal efficiency versus Temperature difference between hot and cold medium for ideal Schmidt cycle (isothermal compression & expansion) for different compression ratios

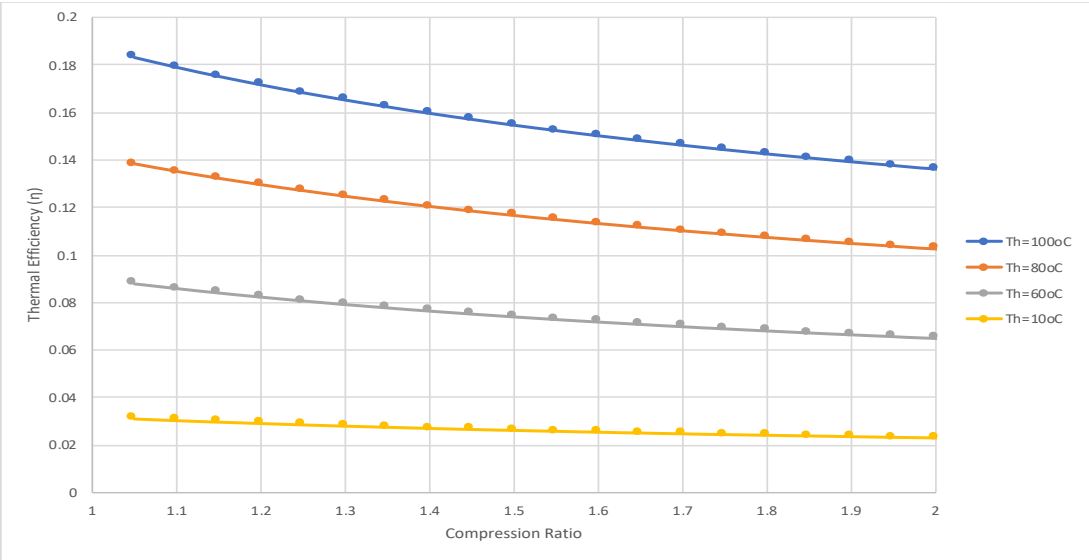

Figure 25. Thermal efficiency versus compression ratio for ideal Schmidt cycle (isothermal compression & expansion) for a range of temperatures for the hot medium [30-100 degrees].

Table 11. Efficiency results for both Carnot and Carlquist for Th between 313 and 373

Tc (K)= 303

Th (K)=	373	363	353	343	333	323	313
Th-Tc (oC or K)=	70	60	50	40	30	20	10
η Carnot	0,18766	0,16528	0,14164	0,11661	0,09009	0,06191	0,03194
ηCarlquist	0,096085	0,0846	0,07252	0,05970	0,04612	0,03170	0,01635

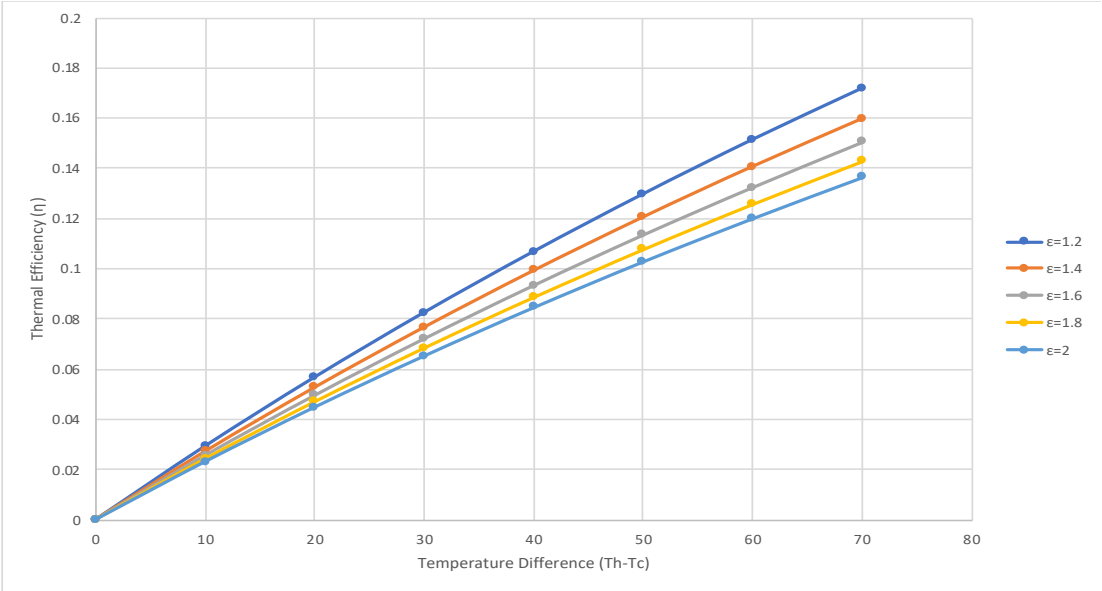

Figure 26. Thermal efficiency versus Temperature difference between hot and cold medium for ideal Schmidt cycle (isothermal compression & expansion) for different compression ratios.

Chapter 4

Rallis Adiabatic and Polytropic Cycle

It was mentioned before that the Stirling cycle was based on the assumption that isothermal expansion and compression processes were unreasonable owing to the poor heat transfer in the working spaces of practical machines. So, it is more reasonable to expect that the expansion and compression processes occur polytropically and in the limit approach adiabatic conditions. Therefore an ideal cycle has been suggested by C. J. Rallis, in which all heat transfer occurred under constant volume conditions and where the expansion & compression process were assumed to be adiabatic. The cycle proposed by C. J. Rallis is generally referred to as the ideal adiabatic Stirling cycle. It has been seen that from cyclic point of view, the ideal adiabatic Stirling cycle model appears to more accurately describing the thermodynamic cycle of practical machines and the results obtained from this cycle were found in conformity with the natural laws and real engine features.

The *P-V* and *T-S* diagram of ideal adiabatic Stirling cycle is shown in Figure 27, where isothermal processes (*1-2′ & 3-4′*) are replaced by isentropic processes (*1-2 & 3-4*) respectively. Here after the compression process, the working fluid is transferred through the cooler at constant volume where its pressure drops to *2′*. The working fluid then passed through the regenerator where its pressure rises to *3′* and finally through the heater at constant volume where the pressure further rises to *3*. Similarly, after the isentropic expansion process, the working fluid is transferred through the heater at constant volume where its pressure rises to *4′* and then passed through the regenerator where its pressure drops to *1′* and finally through the cooler where the pressure further drops to *1*.

However, if it is assumed that expansion & compression processes occur (0<n<k) due to finite heat transfer instead of adiabatic or isothermal then this cycle will be represented by processes *1-2''-2'-3'-3-4''-4'-1'-1* on *P-V* & *T-S* diagram as shown in Figure 27. This cycle is now referred to as the ideal polytropic Stirling cycle and in the limiting case when index of compression/expansion approaches adiabatically (i.e. n=k) it becomes ideal adiabatic Stirling cycle.

The network output obtained from the ideal polytropic cycle is given by:

$$W_{net} = W_E - W_C \tag{45}$$

$$W_{net} = \frac{m\,R}{n-1}[(T_3 - T_{4,,}) - (T_{2,,} - T_1)] \tag{46}$$

The effectiveness (ε) of the regenerator is given by:

$$\varepsilon = \frac{T_{3,} - T_1}{T_3 - T_1} \rightarrow T_{3,} = T_1 + \varepsilon(T_3 - T_1)\ and\ T_{4,} = T_3 \tag{47}$$

The heat (Q_s) provided to the system is given by:

$$\begin{aligned} Q_S &= Q_{3,-3} + Q_{3-4,,} + Q_{4,,-4,} \\ &= m\,C_v\left[(T_3 - T_{3,}) + \frac{k-n}{n-1}\,(T_3 - T_{4,,}) + (T_{4,} - T_{4,,})\right] \end{aligned} \tag{48}$$

By substituting the effectiveness into Qs we get:

$$Q_S = m\,C_v\left[(1-\varepsilon)\cdot(T_3 - T_1) + \frac{k-n}{n-1}\,(T_3 - T_{4,,})\right] \tag{49}$$

Thus, the efficiency of the cycle is:

$$\eta_{Polytropic} = \frac{W_{net}}{Q_s} = \frac{(T_3 - T_{4,,}) + (T_{2,,} - T_1)}{\frac{n-1}{k-1}\,(1-\varepsilon)(T_3 - T_1) + (T_3 - T_{4,,})} \tag{50}$$

From the polytropic relation

$$\frac{T_3}{T_{4,,}} = \left(\frac{V_{4,,}}{V_3}\right)^{n-1} = \frac{T_{2,,}}{T_1} = r^{(n-1)} \tag{51}$$

With r being the compression ratio and by solving with respect to T_3 and $T_{2,,}$ and by substituting them into the thermal efficiency of the cycle, the equation converts to:

$$\begin{aligned} \eta_{Polytropic} &= \frac{(r^{n-1}-1)(T_{4,,}-T_1)}{T_3\left[\frac{n-1}{k-1}\,(1-\varepsilon)\left(1-\frac{T_1}{T_3}\right)+\frac{T_{4,,}}{T_3}\,(r^{n-1}-1)\right]} \\ &= \frac{(r^{n-1}-1)(T_{4,,}-T_1)}{T_3\left[\frac{n-1}{k-1}\,(1-\varepsilon)\eta_{Carnot}+\frac{T_{4,,}}{T_3}\,(r^{n-1}-1)\right]} \end{aligned} \tag{52}$$

Substituting again the $T_{4,,}$ from the polytropic relation and after some algebraic manipulation to finally get the thermal efficiency for the ideal adiabatic Stirling cycle (Rallis Cycle) with regeneration:

$$\eta_{Polytropic} = \frac{(r^{k-1}-1)(1-tr^{n-1})}{\left[\frac{n-1}{k-1}\,(1-\varepsilon)(1-t)r^{n-1}+(r^{n-1}-1)\right]} \tag{53}$$

In case we have ideal regenerator ($\varepsilon = 1$) the above equation reduces to the following:

$$\eta_{Polytropic} = 1 - tr^{n-1} \tag{54}$$

In case we have adiabatic compression and expansion ($n \to k$) the thermal efficiency becomes:

$$\eta_{adiabatic} = \frac{(r^{k-1}-1)(1-tr^{k-1})}{[(1-\varepsilon)(1-t)r^{k-1}+(r^{k-1}-1)]} \tag{55}$$

In addition to the above case, if there is an ideal regeneration, the equation reduces further to:

$$\eta_{Polytropic} = 1 - tr^{k-1} \tag{56}$$

The network in Rallis polytropic cycle with ideal and non-ideal regeneration is given by:

$$W_{net} = mRT_1\left(\frac{r^{n-1}-1}{n-1}\right)\left[\frac{1}{tr^{n-1}}-1\right] \tag{57}$$

Thus the nondimensional Power is given by:

$$\frac{W_{net}}{mRT_1} = \left(\frac{r^{n-1}-1}{n-1}\right)\left[\frac{1}{tr^{n-1}}-1\right] \tag{58}$$

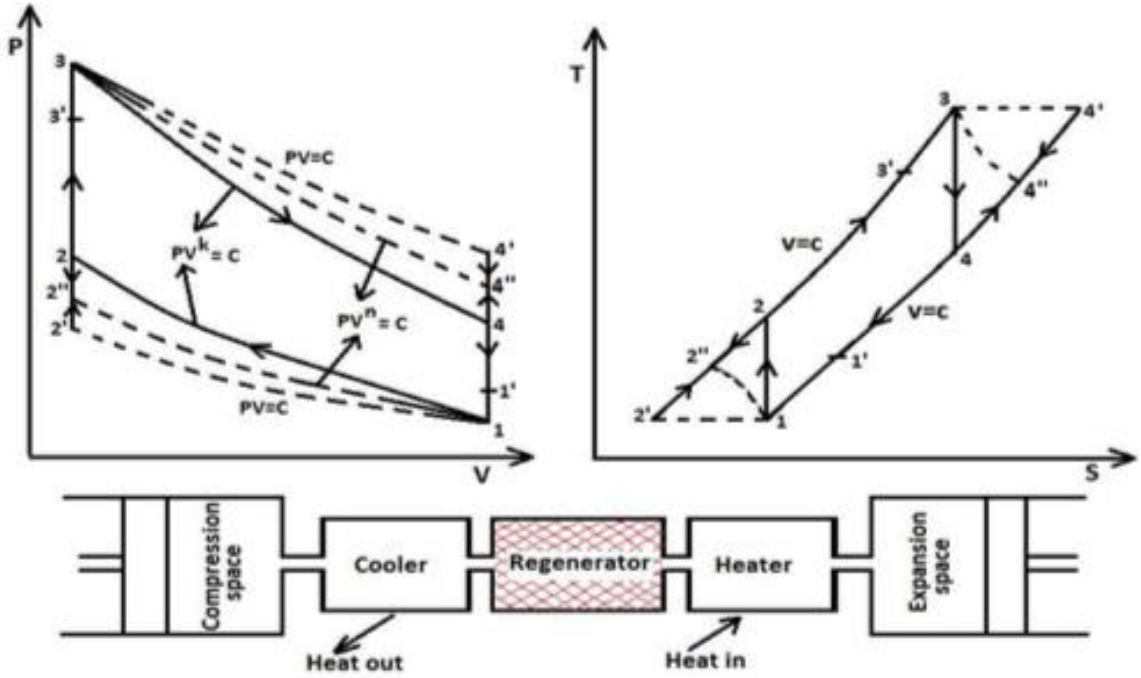

Figure 27. Top left & right: P-V and T-s of Rallis ideal adiabatic (k) and polytropic (n) thermodynamic cycle and bottom: mechanical configuration of ideal Rallis Stirling engine.

4.1. Results and Discussion for Rallis Stirling Engine

Figure 28 shows the effect of regenerator effectiveness in the thermal efficiency of the ideal Rallis Stirling engine with adiabatic compression and expansion as a function of the compression ratio. The cold and hot temperatures of the engine are 30 and 300 degrees respectively while air is the working fluid. It is observed that for ideal regeneration we get a maximum thermal efficiency of 45% at a fairly low compression ratio of 1.1. A continuous decreasing trend is observed with the compression ratio for the case of ideal regeneration while for non-ideal regeneration the efficiency is increasing up to compression ratio of about 1.3 and then decreasing as the compression ratio increases.

The thermal efficiency of the Rallis ideal model with polytropic compression and expansion again the compression ratio for different values of the polytropic index n is presented in Figure 29. It is shown that with the increase of the polytropic index the thermal efficiency is linearly decreasing. The maximum efficiency is 46% for a compression ratio of 1.2 with a very low polytropic index n of 1.05.

Figure 30 shows the effect of the regenerator effectiveness with the compression rate for a constant value of the polytropic index (n=1.1). The trend is decreasing for ideal regeneration while for non-ideal regeneration is increasing with the increase of the compression ratio. It was expected that as the regenerator efficiency decreases the same happens to the thermal efficiency of the cycle.

Figures 31, 36 and 41 show the effect of the polytropic index to the nondimensional power of the Rallis polytropic engine versus the compression ratio for temperatures of the hot medium 300^o, 200^o and 100^o respectively. It is observed that the nondimensional power increases up to specific compression ratio for each value of the polytropic index and then decreases. As the temperature of the hot medium decreases the maximum nondimensional power happens for every polytropic index at a lower compression ratio.

The nondimensional power versus the thermal efficiency for different values of the polytropic index for the Rallis cycle with ideal regeneration are presented in Figures 32, 37 and 42. The nondimensional power increases up to a certain thermal efficiency and then decreases. This happens in all diagrams for all the values of the polytropic index. As

the temperature of the hot medium decreases the maximum in the nondimensional power happens in lower efficiency of the engine.

Figures 33 and 38 show the same results as Figure 28 but with lower temperatures of the hot medium of 200 and 100 degrees respectively. The same trends are observed but with lower thermal efficiencies. In the latter case the thermal efficiency of adiabatic Rallis cycle is 7% with a compression ratio of 1.15 and a regenerator efficiency of 70%. In case of the polytropic Rallis cycle with a polytropic index of 1.1 and a compression ratio of 1.5 the thermal efficiency is 10.5%. For ideal regeneration (100%) in the Rallis polytropic cycle there is no point a polytropic index below 1.25 because the efficiency drops below 10%.

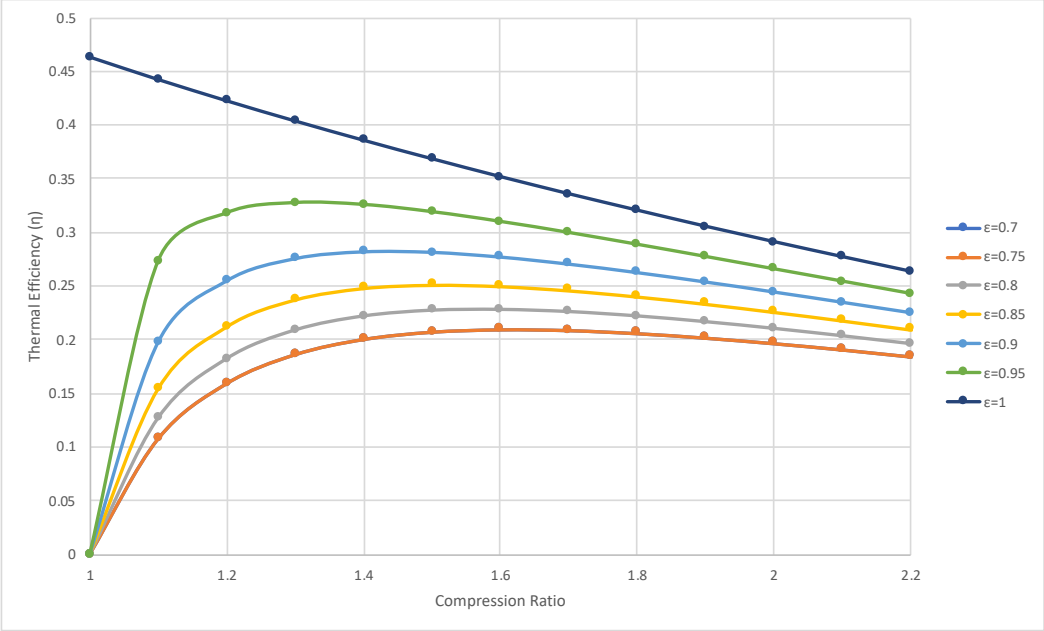

Figure 28. Thermal efficiency versus compression ratio for the adiabatic Rallis Stirling cycle for variable regeneration efficiencies. (Tcold=35° and Thot=300°).

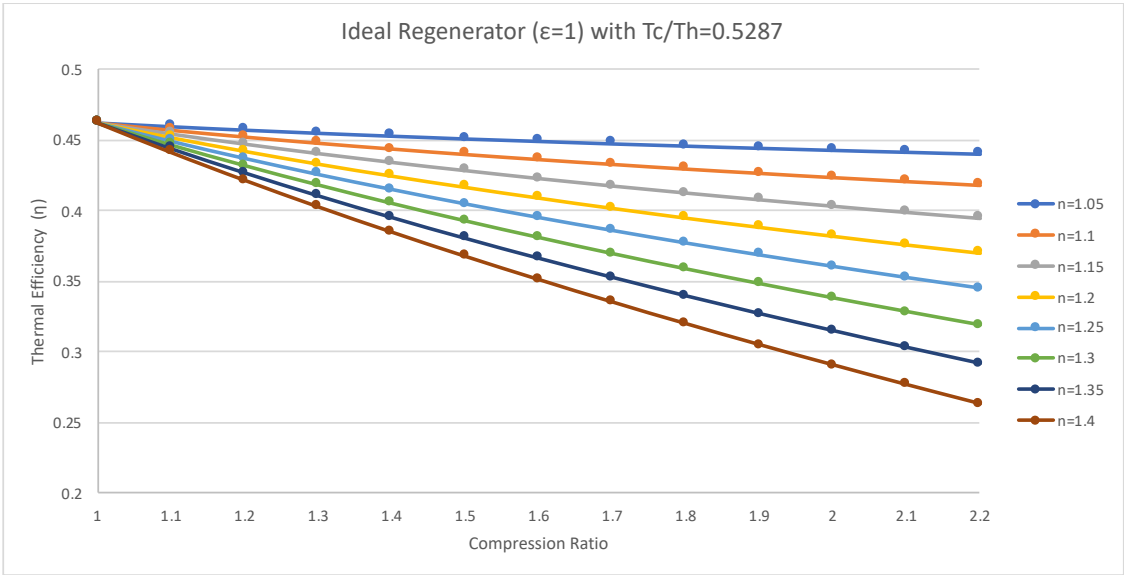

Figure 29. Thermal efficiency versus compression ratio for the polytropic Rallis Stirling cycle for ideal regeneration and variable polytropic index Tcold=35° and Thot=300°.

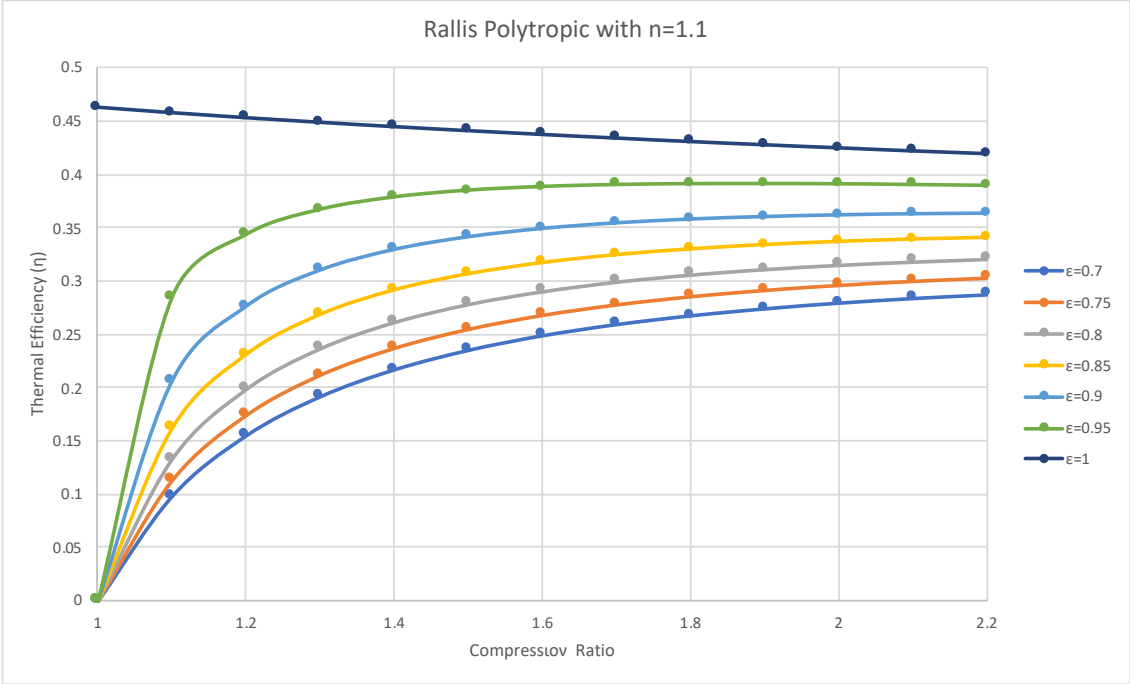

Figure 30. Thermal efficiency versus compression ratio for the polytropic Rallis Stirling cycle for variable regeneration with polytropic index n=1.1 Tcold=35° and Thot=300°).

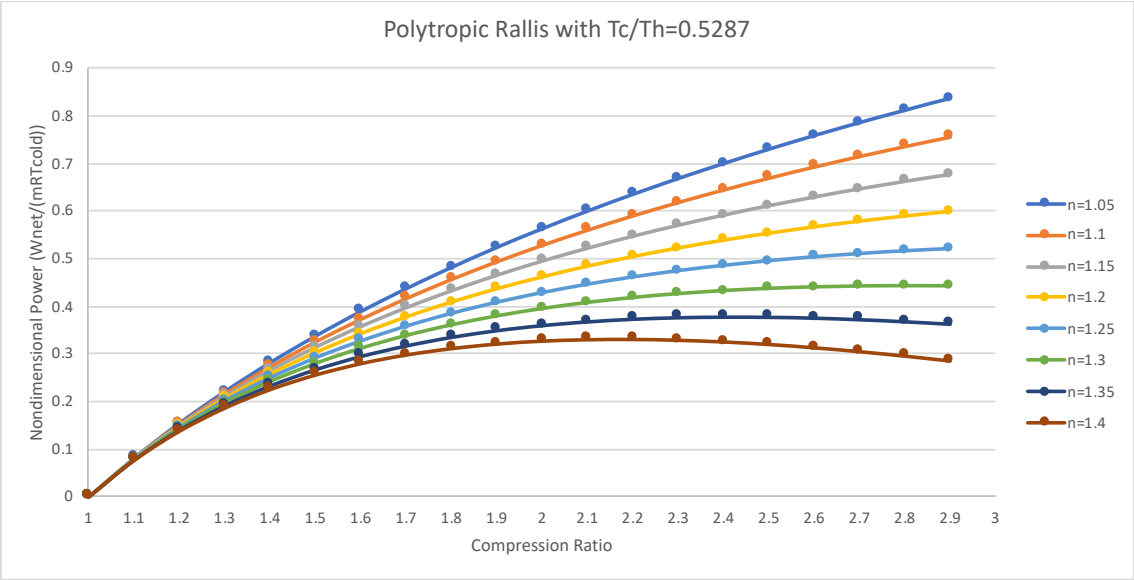

Figure 31. Nondimensional Power versus compression ratio for the polytropic Rallis Stirling cycle for variable polytropic index n Tcold=35° and Thot=300 °.

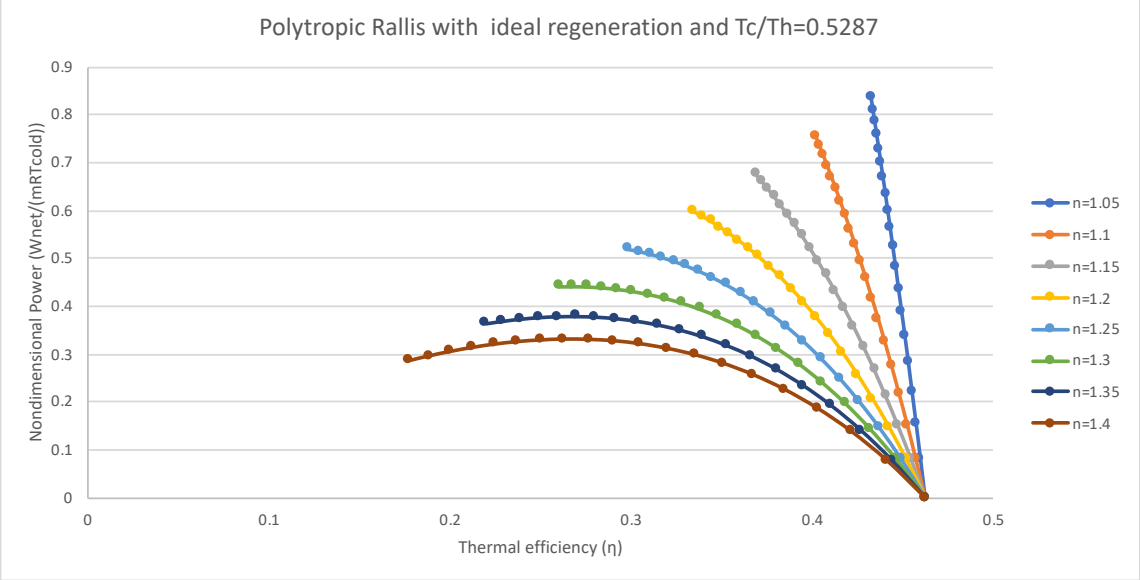

Figure 32. Nondimensional Power versus thermal efficiency for the polytropic Rallis Stirling cycle for variable polytropic index n and ideal regeneration Tcold=35° and Thot=300 °.

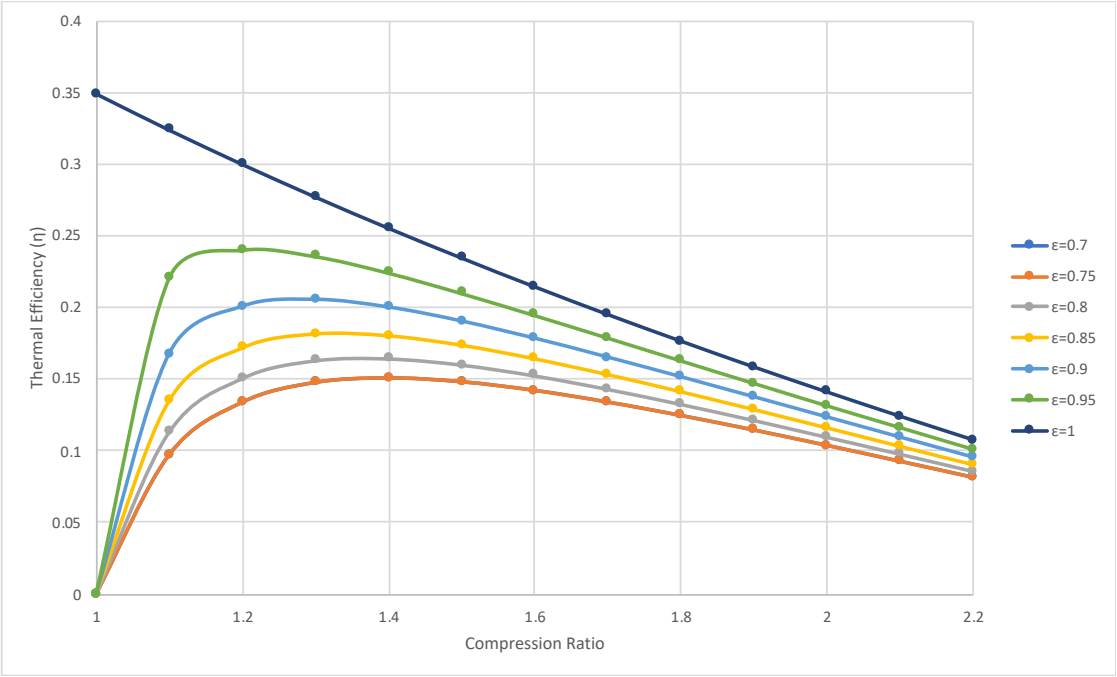

Figure 33.Thermal efficiency versus compression ratio for the adiabatic Rallis Stirling cycle for variable regeneration efficiencies. Tcold=35° and Thot=200 °.

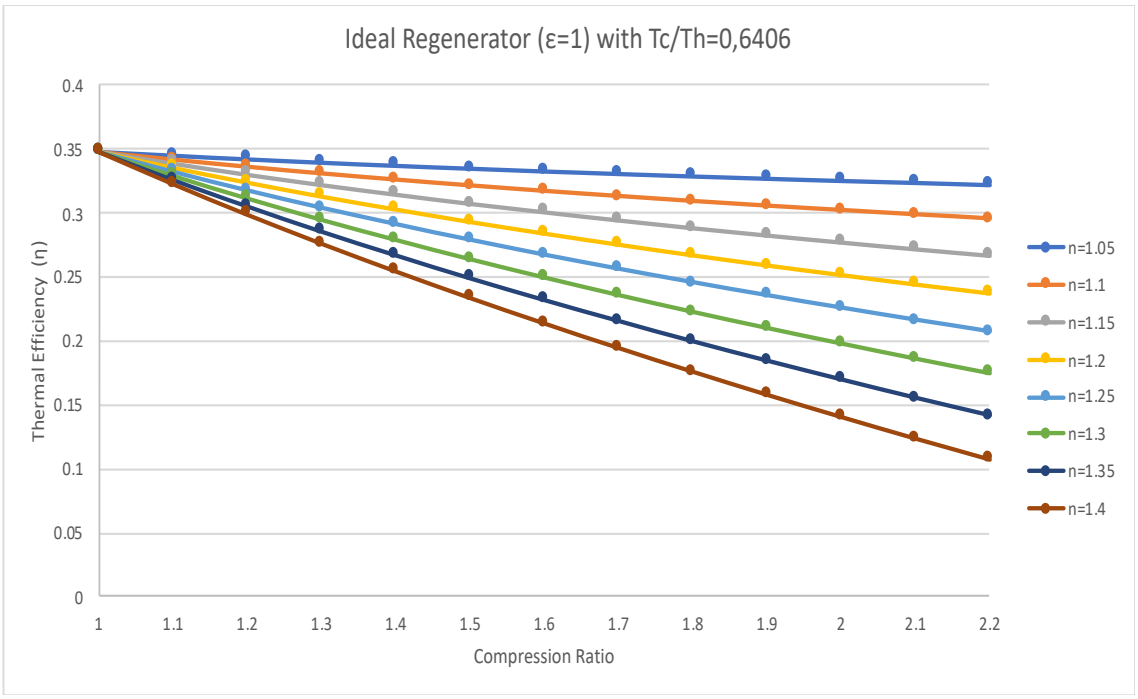

Figure 34. Thermal efficiency versus compression ratio for the polytropic Rallis Stirling cycle for ideal regeneration and variable polytropic index Tcold=35 °and Thot=200 °.

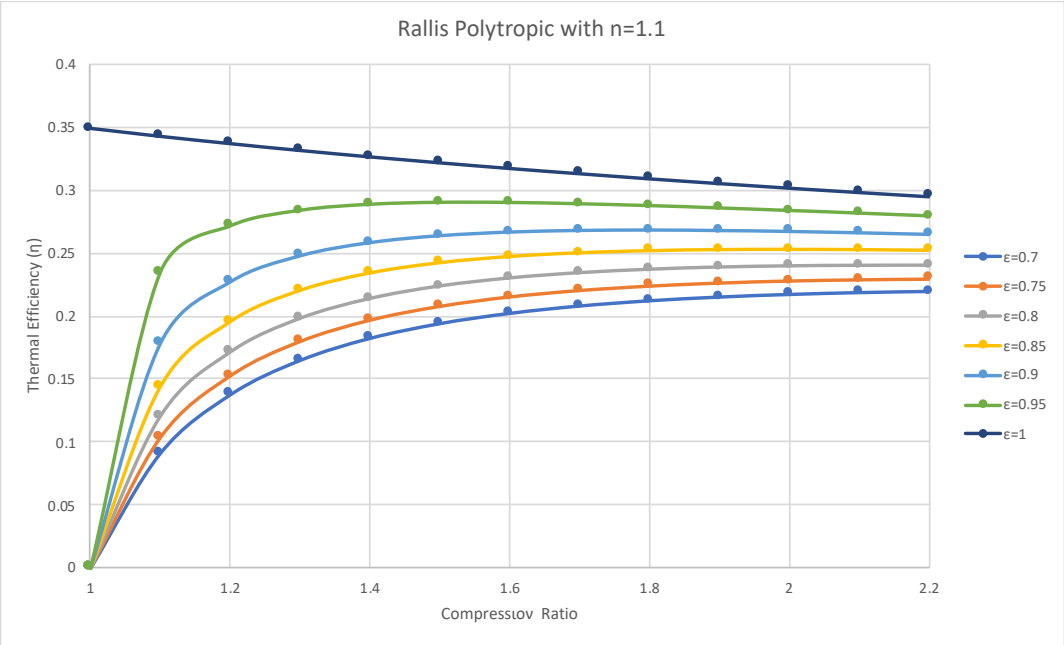

Figure 35. Thermal efficiency versus compression ratio for the polytropic Rallis Stirling cycle for variable regeneration with polytropic index n=1.1 Tcold=35 °and Thot=200 °.

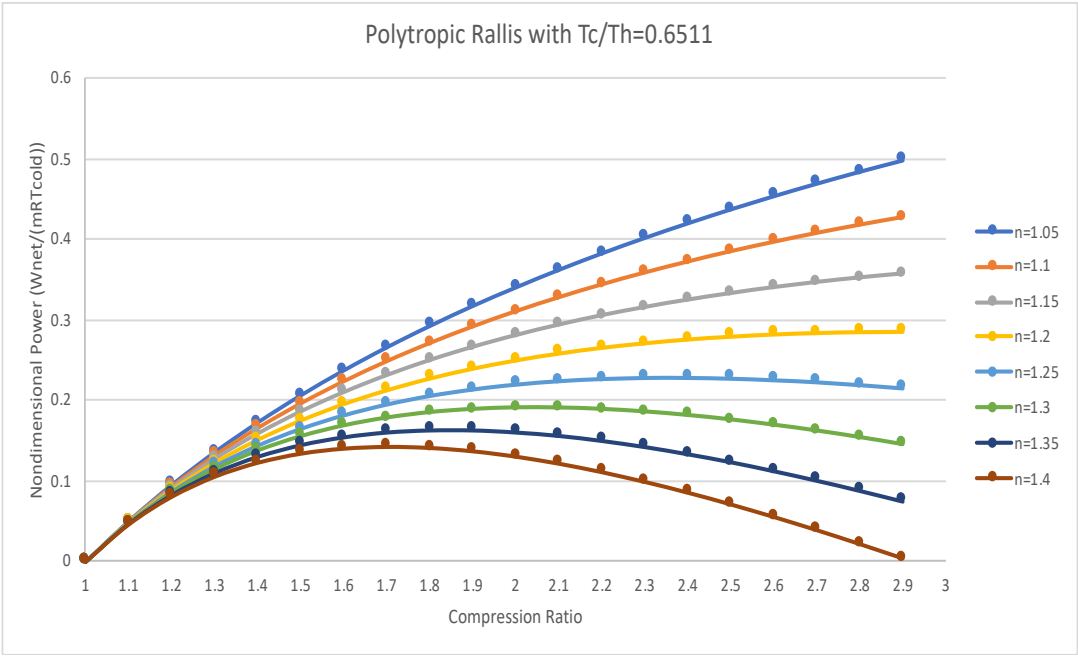

Figure 36. Nondimensional Power versus compression ratio for the polytropic Rallis Stirling cycle for variable polytropic index n Tcold=35 °and Thot=200 °.

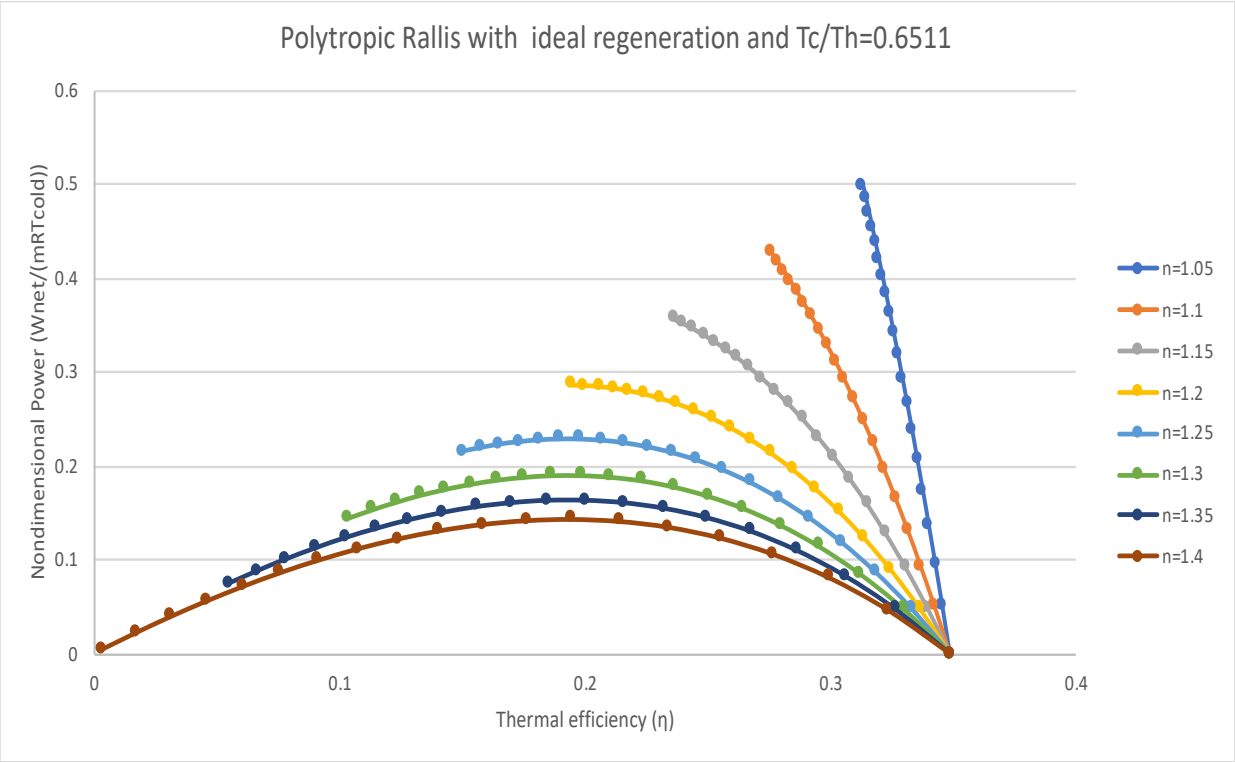

Figure 37. Nondimensional Power versus thermal efficiency for the polytropic Rallis Stirling cycle for variable polytropic index n and ideal regeneration Tcold=35 °and Thot=200°.

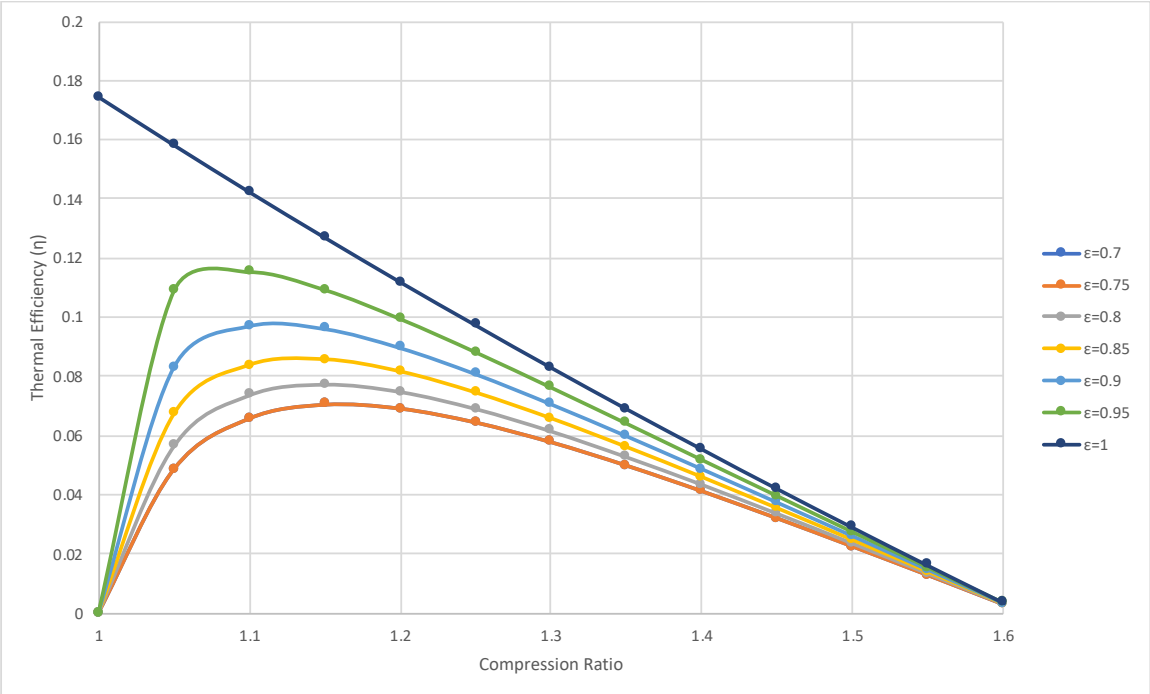

Figure 38. Thermal efficiency versus compression ratio for the adiabatic Rallis Stirling cycle for variable regeneration efficiencies. Tcold=35 °and Thot=100 °.

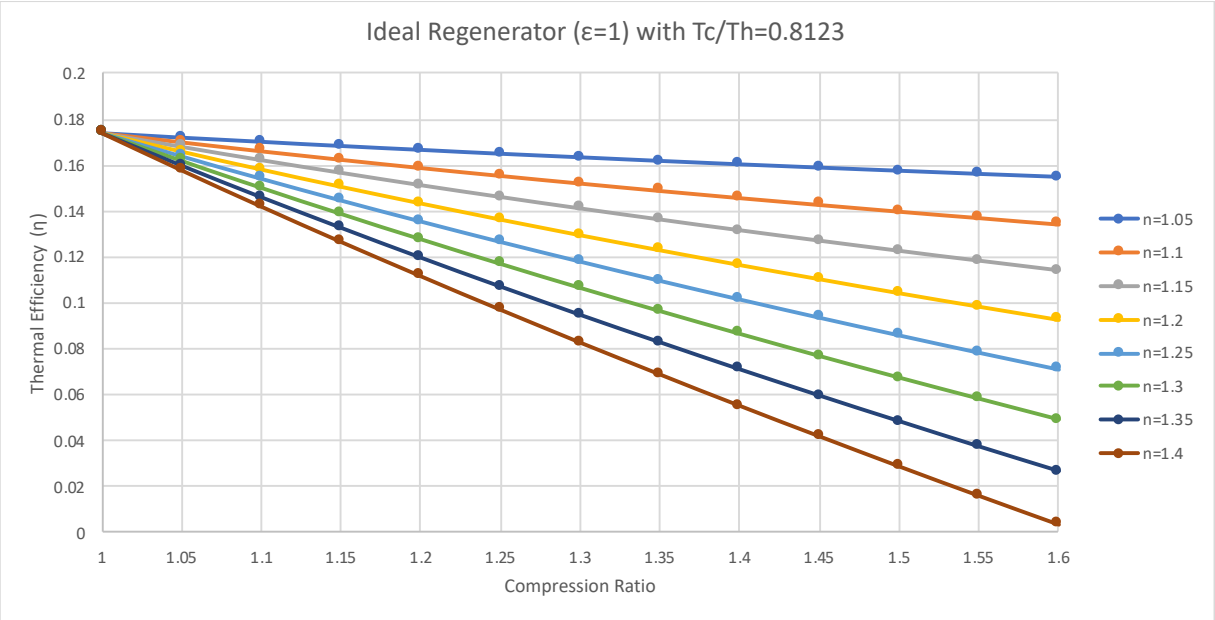

Figure 39. Thermal efficiency versus compression ratio for the polytropic Rallis Stirling cycle for ideal regeneration and variable polytropic index Tcold=35° and Thot=100°.

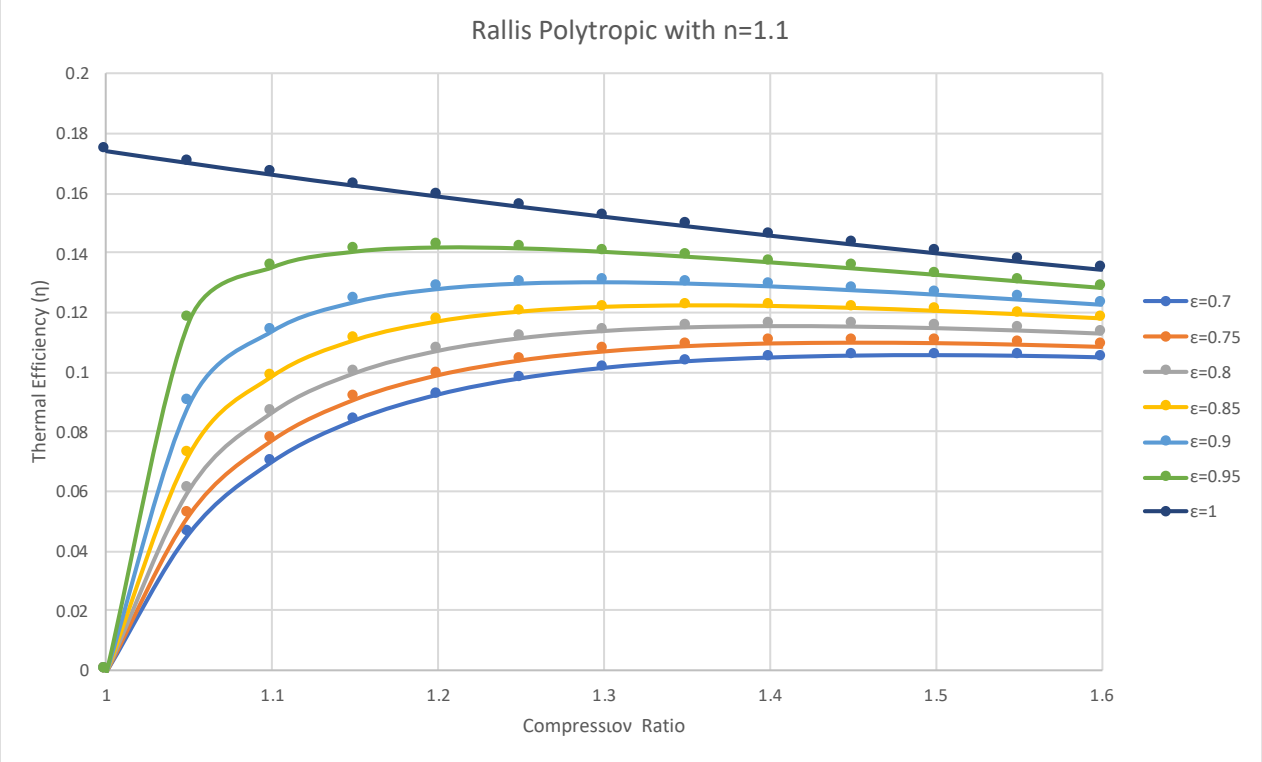

Figure 40. Thermal efficiency versus compression ratio for the polytropic Rallis Stirling cycle for variable regeneration with polytropic index n=1.1 Tcold=35° and Thot=100°.

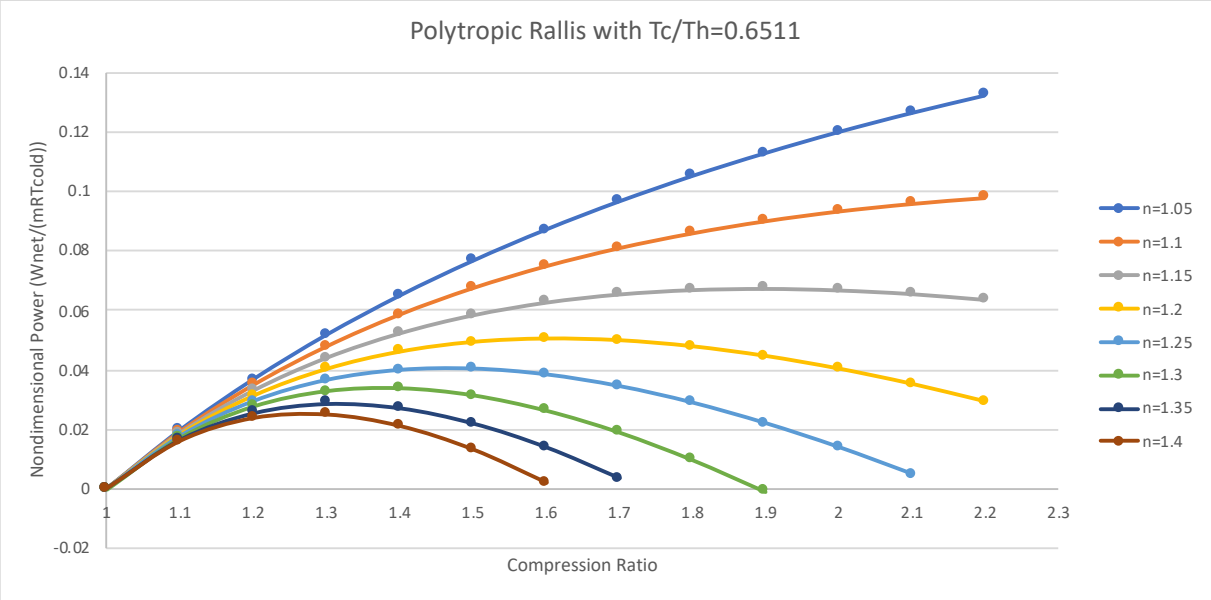

Figure 41. Nondimensional Power versus compression ratio for the polytropic Rallis Stirling cycle for variable polytropic index n Tcold=35 ° and Thot=100 °.

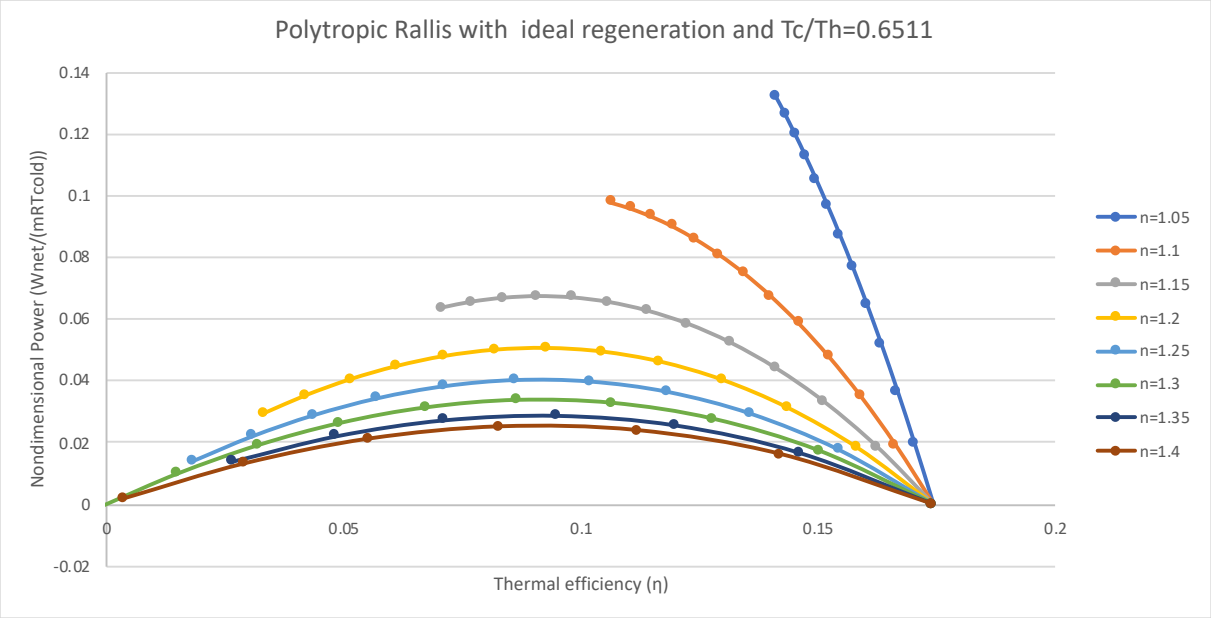

Figure 42. Nondimensional Power versus thermal efficiency for the polytropic Rallis Stirling cycle for variable polytropic index n and ideal regeneration Tcold=35 ° and Thot=100 °.

Summary and Conclusions

Kinetic Stirling engines operating at low and moderate temperature differences have been reviewed and discussed. Most of the Stirling engines were in gamma configurations and typically used ambient pressure air as the working gas. The working temperature differences were around or less than 100°C to 405°C. As the temperature and working pressure were very low, the rotating speeds were typically within 300 rpm. Most of the reported LTD Stirling engines were small in size with power outputs of less than 10 W and efficiencies below 1%. This is mainly because they were manufactured with low-cost materials, assembled with low accuracy and filled with low pressure air.

Several larger LTD Stirling engine prototypes filled with pressurized air showed that it is possible to achieve the power output up to several hundred watts with much higher efficiencies. Although the performance of the developed LTD Stirling engines is relatively limited, the low requirements for heat source temperature and the low costs for manufacturing make them attractive for low temperature heat recoveries, especially when the price is first priority. To achieve a large power and a good efficiency, LTD Stirling engines should be designed with a large size and filled with pressurized working gas.

Most of the kinetic Stirling engines operating at medium temperatures used charged helium or air as working gas. The rotating speed typically ranged from 300 rpm to 600 rpm. The power outputs and efficiencies were both much higher than those of LTD Stirling engines. They have made a compromise between the low performances of LTD Stirling engines and the high prices of the high temperature ones. They have potential applications in solar power generations at low concentration ratios. Compared to advanced and expensive high temperature solar concentration technology, the average concentration solution to temperature levels around 250°C to 450°C has economic advantages and much lower requirements for high temperature materials.

References

Abdullah S. Yousif BF. Sopian K. (2005). Design consideration of low temperature differential double-acting Stirling engine for solar application. *Renewable Energy*, 1923-1941.

Administration, U. E. (2018). *Capacity Factors for Utility Scale Generators Not Primarily Using Fossil Fuels.*

Administration, U. E. (2018). *International Energy Outlook 2018.*

Agency, E. (2018). *Global Energy & CO2 Status Report 2017.* Energy Agency.

Aragn-Gonzlez G, G.-B. M.-P.-G. (2013). Developing and testing low cost LTD Stirling engines. *Rev Mex Fis*, 199-203.

Bancha Kongtragool, S. W. (2005). Optimum absorber temperature of a once-reflecting full conical concentrator of a low temperature differential Stirling engine. *Renewable Energy*, 1671-1687.

C. P. Speer. (2018). *Modifications to Reduce the Minimum Thermal Source Temperature of the ST05G-CNG Stirling Engine.* University of Alberta.

Chen WL. Wong KL. Chang YF. (2014). A computanional fluid dynamics study on the heat transfer characteristics of the working cycle of a low-temperature-differential γ-type Stirling engine. *International Journal of Heat and Mass Transfer*, 145-155.

Chen WL. Wong KL. Chen HE. (2014). An experimental study on the performance of the moving regenerator for a gamma-type twin power piston Stirling engine. *Energy Conversion and Management*, 118-128.

Chen WL. Wong KL. Po LW. (2012). A numerical analysis on the performance of a pressurized twin power piston gamma-type Stirling engine. *Energy Conversion and Management*, 84-92.

Cinar C. Aksoy F. Erol D. (2012). The effect of displacer material on the performance of a low temperature differential Stirling engine. *Interantional Journal of Energy Research*, 911-917.

Cool Energy Inc. (2016). *ThermoHeart.* Retrieved from Ohio: https://www.ohio.edu/mechanical/stirling/engines/ThermoHeart.pdf

Gentherm. (n.d.). *Thermoelectric generators*. Retrieved from Gentherm global power: http://www.genthermglobalpower.com/products/thermoelectric-generators-tegs

Gheith R. Aloui F. Nasrallah SB. (2015). Determination of adequate regenerator for a Gamma type Stirling engine. *Applied Energy*, 272-280.

Haneman D. (1975). *Theory and principles of low-temperature hot air engines fuelled bby solar energy.* US Atomic Energy Communication Contract.

IPCC. (2018). *Global Warming of 1.5oC.*

Isshiki S. Sato H. Konno S. Shiraishi H. Isshiki N. Fujii I. (2008). The experimental study of atmospheric Stirling engines using pin-fin arrays heat exchangers. *Power Energy Systems*, 1198-1208.

Iwamoto I. Toda F. Hirata K. Takeuchi M. Yamamoto T. (1997). Comparison of low and high temperature differential Stirling engines. *Proceedings of the 8th International Stirling Engine Conference*, 29-38.

James R. Senft. (1993). *Ringbom Stirling Engines.* Oxford: Oxford University Press.

Karabulut H, Y. H. (2009). An experimental study on the development of a beta-type Stirling engine for low and moderate temperature heat sources. *Applied Energy*, 68-73.

Karabulut H. Aksoy F. Ozturk E. (2009). Thermodynamic analysis of a beta type Stirling engine with a displacer driving mechanism by means of a lever. *Renewable Energy*, 202-208.

Karabulut H. Cinar C. Ozturk E. Yucesu HS. (2010). Torque and power characteristics of a helium charged Stirling engine with a lever controlled displacer driving mechanism. *Renewable Energy*, 138-143.

Kerdchang P. MaungWin M. Teekasap S. Hirunlabh J. Khedari J. Zeghmati B. (2005). Development of a new solar thermal engine system for circulating water for aeration. *Solar Energy* , 518-527.

Kolin I. (1991). *Stirling motor: history, theory, practice.* Dubrovnik: Inter University Center.

Kolin I. Koscak-Kolin S. Golub M. (2000). Geothermal electrcity production by means of the low temperature difference Stirling engine. *Proceedings World Geothermal Congress Kyushu*, 3199-3203.

Kongtragool B. Wongwises S. (2003). *Theoretical investigation on Beale number for low temperature differential Stirling engines.* Zambia: Proceedings of the 2nd International Conference on Heat Transfer, Fluid Mechanics and Thermodynamics.

Kongtragool B. Wongwises S. (2008). A four power-piston low-temperature differential Stirling engine using simulated solar energy as a heat source. *Solar Energy* , 493-500.

Kongtragool B. Wongwises S. (2008). Testing of a low-temperature differential Stirling engine by using actual solar energy . *International Journal of Green Energy*, 491-507.

Kongtragool B., W. S. (2007). Performance of a twin power piston low temperature differential Stirling engine powered by a solar simulator. *Sol Energy* , 884-895.

O'Hare L.R. (1984). Convection powered solar engine. *US Patent*, 382-453.

R. Fares. (2015). *renewable energy intermittency explained challenges solutions and opportunities.* Retrieved from Scientific American: https://blogs.scientificamerican.com/pluggedin/

Reader G. Hooper C. (1983). *Stirling engines.* London: Spon Press.

Reader G., H. C. (1983). *Stirling engines.* London: Spon Press.

Rizzo J.G. (1995). *The Stirling Engine Manual.* Camden Miniature Steam Service, 3rd edition.

Robson AP. (2007). *A thrid order analysis of a low temperature differential Ringbom-Stirling engine.* Edinburgh: Edinburgh Napier University.

Schmidt G. (1871). Theorie der Lehmannschen calorischen maschine. *Zeit Des Vereines deutsch Ing*, 97-112.

Senft J. (1982). *A simple derivation of the generalized Beale number.* Los Angeles: Proceedings of 17th Intersociety Energy Conversion Engineering Conference.

Senft J. (1982). A simple derivation of the generalized Beale number. *Proceedings of the 17th Intersociety Energy Conversion Engineering Conference*, 1652-1655.

Senft J.R. (1991). *An ultra low temperature differential Stirling engine.* Dubrovnik: Paper ISEC 91032.

Senft J.R. (1993). *Ringbom Stirling Engines.* New York: Oxford University Press.

Shazly JH. Hafez AZ. El Shenawy ET. Eteiba MB. (2014). Simulation, design nad thermal analysis of a solar Stirling engine using MATLAB. *Energy Conversion and Management*, 626-639.

Spencer L.C. (1989). A comprehensive review of small solar-powered heat engines: Part III,. *Solar Energy 43*, 211-225.

Sripakagorn A. Srikam C. (2011). Design and performance of a moderate temperature difference Stirling Engine. *Renewable Energy*, 1728-1733.

Tavakolpour AR. Zomorodian A. Golneshan AA. (2008). Simulation, construction and testing of a two-cylinder solar Stirling engine powered by a flat-plate solar collector without regenerator. *Renewable Energy*, 77-87.

Thombare DG. Verma SK. (2008). Technological development in the Stirling cycle engines. *Renewable & Sustainable Energy Reviews*, 1-38.

Walker G. (1979). Elementary design guidelines for Stirling engines. *Proceedings of the 14th Intersociety Energy Conversion Engineering Conference*, 1066-1068.

West C. (1981). Theoretical basis for the Beale number. *Proceedings of the 16th Intersociety Energy Conversion Engineering Conference*, 1886-1887.

West CD. (1986). *Principles and applications of Stirling engines.* New York: Van Nortrand Reinhold Company Inc.

White E.W. (1983). Solar heat engines. *US Patent*, 414-814.